FRONT MATTER

Title: IL-7/IL-15/IL-21 cytokine-fusion scaffold generates highly functional CAR-T cells enriched in long-lived T memory stem cells

Authors: Erin B. Cole[1], Sara Lamcaj[1], Agnes V. Sydenstricker[1], Adilyn G. Voss[1], Christopher R. Hiner[1], Hong B. Hur[4], Manoj Kandpal[4], Natalia Valderrama Pena[2], Jian Hua Zheng[1], Ying Xiong[3], Zhongyu Zhu[3] Cheng Cheng Zhang[5], Niraj Shrestha[2], Boro Dropulic[3], Hing C. Wong[2], Harris Goldstein[1,6,*]

Affiliations

[1]Department of Microbiology and Immunology, Albert Einstein College of Medicine; Bronx, NY, 10461, USA.

[2]HCW Biologics Inc.; Miramar, FL, USA

[3]Caring Cross; Gaithersburg, Maryland, USA.

[4]RUH Bioinformatics, Center for Clinical and Translational Science, Rockefeller University Hospital; New York, NY 10065.

[5]Department of Physiology, University of Texas Southwestern Medical Center; Dallas, TX 75390, USA.

[6]Department of Pediatrics, Albert Einstein College of Medicine; 1300 Morris Park Ave, Bronx, NY, 10461, USA.

***Corresponding Author**. Email: harris.goldstein@einsteinmed.edu

Short Title: IL-7/IL-15/IL-21 scaffold produces CAR-TSCM cells

Teaser: Scaffold-linked IL-7/IL-15/IL-21 treatment generates highly functional CAR-T cells substantially enriched for T memory stem cells.

ABSTRACT

Functional persistence of chimeric antigen receptor T-cells (CAR-Ts) is limited by conventional CAR-T manufacturing utilizing anti-CD3/CD28 (αCD3/28) stimulation, which generates terminally differentiated and shorter-lived CAR-Ts. We demonstrated HCW9206, a unique protein scaffold linking IL-7, an IL-15/IL-15Rα complex, and IL-21, generates CAR-Ts without requiring αCD3/28 activation which are highly enriched in long-lived T-memory stem cells (T_{SCM}) (> 50%) and display potent activity across distinct disease models, HIV-1 or B cell leukemia. In a humanized mouse HIV infection model, HCW9206-generated anti-HIV-duoCAR-Ts suppressed viremia more effectively than αCD3/28-generated anti-HIV-duoCAR-Ts. In a xenograft leukemia mouse model, a recall proliferative response and complete clearance of leukemia rechallenge was displayed by HCW9206-generated, but not by αCD3/28-generated anti-CD19-CAR-Ts. HCW9206, a first-in-class cytokine-scaffold-based platform, enables production of more potent CAR-T-based immunotherapies by generating a CAR-T-population which is highly functional and also markedly enriched for long-lived T_{SCM}. This strategy is broadly applicable to increase persistence and functionality of CAR-Ts, enhancing their efficacy for treating infectious disease and cancer.

MAIN TEXT

Introduction

Chimeric antigen receptor T-cell therapy (CAR-T) has revolutionized the cancer immunotherapy field with FDA approval of five CAR-T therapeutics for the treatment of leukemia, lymphoma, and, more recently, multiple myeloma (*1-8*). CAR-T therapy has been extended beyond cancer therapy into the treatment of chronic infectious diseases, particularly as a treatment to provide a functional cure for HIV-1 in people living with HIV (PLWH). However, the effectiveness of CAR-Ts to persistently suppress HIV faces many challenges, including the high mutation rate of reverse transcriptase, which enables the emergence of immune escape viral variants in parallel with recurrent viremia after the cessation of antiretroviral therapy (ART) from a population of latently infected cells (*9-12*). To circumvent immune escape by HIV, these HIV-targeting CAR-T cells must be engineered to recognize highly conserved epitopes in the HIV-1 envelope glycoprotein gp120 (Env) expressed on the surface of HIV-infected cells. First-generation anti-HIV-1 CAR-T cells targeting the CD4 binding domain of HIV-1 gp120 with a human CD4 extracellular domain fused to a CD3ζ signaling domain only minimally controlled HIV-1 infection due to the limited T-cell signaling delivered by CARs containing only the CD3ζ TCR signaling domain, and the unintended consequence of the CD4-based CAR conferring $CD8^+$ T cells with susceptibility to HIV infection (*13-15*). We previously reported overcoming these limitations by constructing duoCAR-T cells, second-generation CAR-T cells expressing two independent CAR domains targeting two highly conserved HIV-Env epitopes linked to CD3ζ and 4-1BB costimulatory signaling domains; the anti-HIV CAR molecules, mD1.22-CAR and m36.4-CAR, target the highly conserved CD4 and CCR5 co-receptor binding sites of HIV, respectively (*16, 17*).

Although these multi-specific anti-HIV duoCAR-T cells display potent suppression of HIV infection in vivo, to date, none of the tested anti-HIV CAR-T cells have demonstrated long-term HIV suppression following discontinuation of ART (*13, 14, 18-20*). We hypothesized that one factor reducing the functional persistence of CAR-T cells may be the standard method used for activating T cells to enable their transduction by CAR-encoding LV, which involves T-cell activation through TCR signaling with antibodies to CD3 and CD28 (αCD3/28). While this method enables highly efficient LV transduction, it also generates a more differentiated CAR-T cell product that correlates with reduced persistence of cytotoxic function (*21, 22*). Previous studies of CD19-CAR-T cell therapy have shown that patients with the best clinical outcomes often have CAR-T cells with a less differentiated, early memory phenotype, particularly T memory stem cell (T_{SCM}) cells, which are characterized by the expression of markers such as $CD45RO^-$, $CCR7^+$, $CD95^+$, $CD45RA^+$, $CD62L^+$, $CD27^+$, $CD28^+$, and IL-$7R\alpha^+$ (*23, 24*). The T_{SCM} subset represents the earliest stage of T-cell differentiation following naïve T-cells (T_N), and consequently, both T-cell subpopulations share many functional and phenotypic characteristics, such as expressing the same T-cell marker, CCR7, but not CD45RO ($T_{N/SCM}$: $CD45RO^-CCR7^+$). T_{SCM} can be distinguished from T_N by their expression of CD95; thus, T_{SCM} are characterized as $CD45RO^-$ $CCR7^+CD95^+$. This very early stage of T-cell differentiation confers the ability to differentiate into diverse T-memory progeny and exhibit self-renewal, high proliferation, and long-term survival in vivo (*25, 26*). This T_{SCM} phenotype is crucial for generating the most effective HIV-specific CAR-T cells, as the continuous presence of functional anti-HIV CAR-T cells is necessary for sustained HIV suppression. This is important to prevent viral rebound from long-lived latently infected cell populations that can reintroduce dispersed HIV infection after ART is stopped (*3, 17, 25*).

However, the generation of significant populations of T_{SCM} CAR-T cells using standard approaches is hindered by the rarity of T_{SCM} populations, which comprise only 2-3% of circulating T cells (*25*). While this can be circumvented by generating CAR-T cells from highly purified T_N or T_{SCM} cells, obtaining these T_{SCM} cells requires starting with a very large population of T cells. In turn, the generated CAR-T_{SCM} cells display reduced cytotoxic function and cytokine production (*27*). An alternative protocol generated significant populations of T_{SCM} CAR-T cells by stimulating highly purified naïve $CD8^+$ T cells with soluble αCD3 antibody alone, followed by transduction with a CAR-encoding LV and treatment with IL-7 and IL-15 for 4 weeks of culture (*28*). While culturing CAR-T cells with IL-7, IL-15, and IL-21 after generation by αCD3/28 stimulation was reported to increase the population of CAR-T cells displaying naive and early memory phenotypes compared to culture with IL-2, this study did not specifically evaluate the generation of T_{SCM} CAR-T cells (*29*). Other methods have been employed to prolong the persistence of CAR-T cells, including blocking T-cell differentiation through activation of Wnt signaling (*30*) and generating CAR-T cells that preserve stem-like memory activity through IL-10 immunosuppressive signaling (*31*). In this study, we demonstrate that HCW9206, a novel soluble tissue-factor fusion molecule that links IL-7, an IL-15/IL-15Rα sushi domain complex, and IL-21 to activate and expand memory-like natural killer (NK) cells (*32*), enables highly efficient T cell transduction with CAR-encoding LV to generate both HIV- and CD19-specific CAR-T cells. These CAR-T cells are comprised of both a large population of CAR-T_{SCM} and sufficient CAR-T effector cells to effectively suppress HIV infection or eliminate $CD19^+$ tumor cells. The generation of CAR-T cells by HCW9206 treatment represents a marked improvement over CAR-T cell production by standard αCD3/28 activation, as they consist of a

several-fold higher fraction of CAR-$T_{SCM,}$ enabling them to display more persistent functional activity and potent effector functions.

Results

Treatment with HCW9206, a scaffold protein linking IL-7, an IL-15/IL-15Rα sushi domain complex and IL-21, stimulates proliferation of $CD8^+$ T cells particularly those with a T_{SCM} phenotype

To deliver optimal cytokine support for expanding anti-tumor memory-like NK cells ex vivo, we developed a multifunctional fusion molecule, HCW9206, which links human IL-7, an IL-15/IL-15Rα sushi domain complex (IL-15SA), which functions as an IL-15 superagonist (*33*), and IL-21 (**Figure 1A**). We previously verified the biological activity of the HCW9206-linked IL-15/IL-15Rα sushi domain, IL-7, and IL-21 by demonstrating their capacity to drive proliferation of the cytokine-dependent cell lines CTLL-2, 2E8, and B9, respectively (*32*). To further demonstrate the biological activity of the cytokines linked to HCW9206 in primary T cells, we assessed their ability to activate STAT5 and STAT3, transcription factors which are phosphorylated during the JAK/STAT signaling cascade; STAT5 phosphorylation is initiated by IL-7 and IL-15 and, to a lesser extent, IL-21 and STAT3 phosphorylation is induced by IL-7, IL-15, or IL-21 (*34*). After treatment of donor-derived $CD8^+$ T cells with HCW9206 (100 nM) or with IL-7, IL-15, or IL-21 (1 nM), STAT5 phosphorylation was induced by IL-7, IL-15, and HCW9206, but not by IL-21 (**Figures 1B and 1C**). 100nM of HCW9206 was identified as an optimal dose through a titration analysis that evaluated proliferation of CAR-T cells and generation of CAR-T_{SCM} cells (**Figures S1A-B**). STAT3 was phosphorylated by treatment with HCW9206, IL-7, IL-15 and IL-21 cytokines, whereas STAT5 was not significantly

phosphorylated after IL-21 treatment, corresponding to its primary induction of STAT1 and STAT3 phosphorylation (**Figures 1B and 1D**) (*34*). These data indicate that HCW9206 induces phosphorylation of both STAT5 and STAT3, consistent with the activities of its linked cytokines.

We compared the capacity of HCW9206 treatment to induce proliferation of T-cells to αCD3/28 stimulation with added IL-2 by treating Cell Trace Violet (CTV)-stained donor human T-cells with HCW9206 or αCD3/28 for 7 days. Proliferation evaluated by flow cytometric quantification of dye dilution demonstrated that the fraction of CD8 T-cells that underwent proliferation following HCW9206 treatment (86.3% ± 7.2%) was comparable to that observed with αCD3/28 treatment (97.8% ± 1.2%) (**Figures 1E, 1F, and 1G**). However, the fraction (92.1% ± 3.8%) of CD8 T-cells in the $T_{N/SCM}$ memory quadrant ($CD45RO^{-}CCR7^{+}$) that underwent proliferation after HCW9206 treatment was significantly higher ($p = 0.0021$) than the fraction of $CD45RO^{-}CCR7^{+}$ CD8 T-cells (43.7% ± 18.5%) that proliferated in response to anti-CD3/28 stimulation (**Figure 1G**) This likely results from the CD8 T-cells that proliferate in response to αCD3/28, downregulating CCR7, with the remaining small population in that quadrant being naive T cells rather than T_{SCM}, which makes them less prone to proliferation. These results indicate that HCW9206 promotes the proliferation of CD8 T cells, but unlike αCD3/28 treatment, it also preferentially induces the proliferation of T_{SCM}-like cells, consistent with previous reports that IL-7 and IL-15, homeostatic cytokines, can drive the proliferation of T_{SCM} cells, but not T_N (*25*).

The treatment of human T-cells with HCW9206 enables highly efficient LV transduction and generation of CAR-T cells with a predominant T_{SCM} phenotype

We hypothesized that we could enhance the persistence of CAR-T cells by developing a cytokine-based alternative to the standard CAR-T cell generation method of αCD3/αCD28 activation to enable the generation of CAR-T cells with greater proliferative and self-renewal capacity. Previous studies reported that treatment with cytokines such as IL-7 or IL-15 would enable T cells to be transduced with LV to generate early memory T cells engineered to express defined TCR alpha and beta chains or CD19-targeting CAR that display improved therapeutic activity (*21, 35, 36*). We examined whether treatment with a combination of IL-7, IL-15SA, and IL-21 linked by a scaffold would confer susceptibility to LV transduction on T cells and enable the generation of CAR-T cells with a predominant T_{SCM} phenotype, as well as CAR-T cells with potent effector activity. We compared the CAR-T cells generated from donor-derived T-cells transduced with a lentiviral vector expressing an anti-HIV duoCAR (**Figure 2A)** (*16*). Cells were activated either with standard αCD3/αCD28 activation (αCD3/28) in the presence of recombinant human cytokines (e.g., IL-2) or with HCW9206 treatment alone (**Figure 2B**). Comparable transduction efficiency with the duoCAR LV was observed for T cells after either standard αCD3/28 stimulation and IL-2 treatment (duoCAR-$T_{\alpha CD3/28}$), αCD3/28 stimulation followed by treatment with IL-15 or IL-7, IL-15 and IL-21 or HCW9206 (duoCAR-$T_{HCW9206}$) treatment as indicated by expression of the two duoCAR gp120 binders, m36.4 and mD1.22 (**Figures 2C, 2D and S2A**). However, the fraction of duoCAR-T cells that were T_{SCM} cells was ~14-fold higher in the duoCAR-$T_{HCW9206}$ cell population (58.7% ± 8.5%) compared to the duoCAR-$T_{\alpha CD3/28}$ cell population (4.1% ± 2.9%), as indicated by their expression of T_{SCM} phenotype markers, $CD45RO^{-}CCR7^{+}CD95^{+}$ ($p < 0.0001$) (**Figures 2E, S2B, S2C and S2D**). We observed that T_{SCM} expansion occurred with IL-15 treatment alone but not with αCD3/28 stimulation combined with IL-15 or with a mix of IL-7, IL-15, and IL-21. This is likely a

consequence of the potent αCD3/28 stimulation signal driving differentiation of T_{SCM} cells, overriding the capacity of IL-15 alone or in combination with IL-7 and IL-21, to sustain early-memory T_{SCM} cells (*37*). In contrast, IL-15 alone supported T_{SCM} enrichment, but to a significantly lesser extent than treatment with a combination of IL-7, IL-15 and IL-21 delivered by HCW9206 treatment ($p = 0.0269$). We then evaluated the capacity of these T_{SCM} CAR-T cells to display the characteristic capacity of T_{SCM} cells to generate diverse T-memory cell progeny in response to antigen stimulation (*25, 38*). We compared the memory phenotype of duoCAR-$T_{HCW9206}$ or duoCAR-$T_{\alpha CD3/28}$ cells before and after gp120-stimulation for 4-days by co-culture (2:1 E:T ratio) with HEK-293T cells expressing the HIV-1 envelope protein gp120 (293T-gp120 cells). After gp120 stimulation, there was a shift of the predominant duoCAR-$T_{HCW9206}$ phenotype from T_{SCM} (59.8% ± 7.7%) to the more differentiated T_{CM} memory phenotype (50.3% ± 3.7%) with a commensurate reduction in the T_{SCM} population to 25.5% ± 3.0% (**Figure 2F**).

We further evaluated the capacity of HCW9206 treatment to generate CAR-T cells by investigating its ability to produce CD19-specific CAR-T cells (**Figure 3A**). As observed for duoCAR-T cell production, while HCW9206 treatment generated levels of CD19-CAR-T cells (CD19-CAR-$T_{HCW9206}$ cells) comparable to the standard αCD3/28 method (CD19-CAR-$T_{\alpha CD3/28}$ cells) (**Figures 3B and S3A**), the phenotype of CAR-T cells that was T_{SCM} ($CD45RO^-$ $CCR7^+CD95^+$) was ~12-fold higher compared to CD19-CAR-$T_{\alpha CD3/28}$ cells ($p < 0.0001$) (**Figures 3C, 3D and S3B**). Importantly, we also determined that at an equimolar concentration (1 nM), HCW9206 treatment led to a significant ($p = 0.03$), almost 2-fold, increase in the population of $CD45RO^-CCR7^+CD95^+$ CD19-CAR-T_{SCM} cells (69.60% ± 14.9%) compared to IL-7 stimulation alone (37.58% ± 6.6%) (**Figure 3E**). The T_{SCM} phenotype of these $CD45RO^-CCR7^+CD95^+$ CD19-CAR-$T_{HCW9206}$ cells was further confirmed by their co-expression of several markers

associated with T-stemness, including CCR7, CD45RA, CD27, and CD95 **(Figures 3C and S3C)**, absence of expression of the T-virtual memory marker (T_{VM}), NKG2A (**Figure S3D**), and expression of the T-cell progenitor-associated transcription factor TCF-1 (**Figure S3D**). As observed for the duoCAR-$T_{HCW9206}$ cells, we observed a marked shift for the T_{CM} phenotype in the CD19-CAR-$T_{HCW9206}$ cells after antigen stimulation by CD19 delivered by a 4-day culture with $CD19^+$ NALM-6 cells, with the average population of T_{SCM} decreasing from 58.7% ± 4.0% to 4.4% ± 1.9% while the average population of T_{CM} increased from 20.1% ± 2.7% to 74.2% ± 3.1% (**Figure 3F**). Taken together, these data demonstrate that HCW9206 treatment generates CAR-T cells that are markedly enriched for early memory T_{SCM} cells.

CAR-T cells generated by HCW9206 treatment or αCD3/28 activation display comparable in vitro functional activity

We compared the functional capacity of duoCAR-$T_{HCW9206}$ cells and duoCAR-$T_{\alpha CD3/28}$ cells to suppress infection by an HIV-1 infectious molecular clone (IMC) expressing a *Renilla* luciferase reporter gene (HIV-LucR) as previously described (*16, 17*). PHA-activated $CD4^+$ T-cells were infected with HIV-LucR expressing either the BaL or JRCSF Env glycoprotein, cultured with the indicated syngeneic duoCAR-T cells, and the level of HIV infection was determined by quantifying luciferase activity several days later. DuoCAR-$T_{HCW9206}$ and duoCAR-$T_{\alpha CD3/28}$ cells exhibited comparable in vitro suppression of HIV-1 infection in a dose-dependent manner, achieving > 90% suppression at a 1:10 E:T ratio following infection with an IMC expressing the JRCSF envelope (**Figures 4A**) and > 67% suppression with an IMC expressing Bal envelope (**Figures 4B**). Similarly, CD19-CAR-$T_{HCW9206}$ and CD19-CAR-$T_{\alpha CD3/28}$

cells exhibited equivalent cytotoxicity against $CD19^+$ tumor cell lines, including Raji (**Figure 4C**) and NALM-6 (**Figure 4D**).

We further evaluated the function of the HCW9206 and αCD3/28-generated CAR-T cells by determining their cytokine production after activation with their cognate antigens. DuoCAR-$T_{HCW9206}$ cells produced significantly higher levels of TNFα ($p = 0.0172$) and IFNγ ($p = 0.0016$) after incubation with 293T-gp120 cells compared to duoCAR-$T_{\alpha CD3/28}$ cells (**Figure 4E and Figure S4A**), due to increased production by the duoCAR-$T_{HCW9206}$ cell T_{EM} population of IFNγ ($p = 0.001$) (**Figure 4F**) and TNFα ($p = 0.0002$) (**Figure 4G**). Similarly, CD19-CAR-$T_{HCW9206}$ cells displayed increased production of IFNγ ($p = 0.0107$) and TNFα ($p = 0.0001$) after incubation with target NALM-6 cells compared to CD19-CAR-$T_{\alpha CD3/28}$ cells (**Figure 4H**), likely due to increased production by the CD19-CAR-$T_{HCW9206}$ cell T_{EM} population of IFNγ ($p = 0.001$) (**Figure 4I**) and by both the CD19-CAR-$T_{HCW9206}$ cell T_{EM} ($p = 0.0534$) and T_{SCM} ($p = 0.0043$) populations of TNFα (**Figure 4J**). Furthermore, we observed significantly lower expression of the exhaustion markers LAG3 and TIM3 in duoCAR-$T_{HCW9206}$ cells compared to duoCAR-$T_{\alpha CD3/28}$ cells, both at baseline and after 24 hours of stimulation with 293T-gp120 cells (**Figure S4B-C**), indicating that HCW9206 stimulation does not drive a dysfunctional activation state. Overall, these findings demonstrate that CAR-$T_{HCW9206}$ cells have cytotoxic functions similar to or superior to those of CAR-$T_{\alpha CD3/28}$ cells, while also exhibiting an enriched early memory T_{SCM} phenotype.

Anti-HIV duoCAR-$T_{HCW9206}$ display increased T_{SCM} transcriptional programming and effector signatures compared to duoCAR-$T_{\alpha CD3/28}$

To further evaluate the differences between anti-HIV duoCAR-T generated by standard αCD3/28 stimulation and HCW9206 treatment, we compared their transcriptomes with or without stimulation with 293T-gp120 cells. $CD8^+$ duoCAR-$T_{\alpha CD3/28}$ cells and duoCAR-$T_{HCW9206}$ cells generated from two donors were either cultured with 293T cells (unactivated) or cultured with 293T-gp120 cells (activated) for 16 hours, purified by flow cytometric sorting, and their transcriptomes (N = 2 biological replicates) were evaluated by bulk RNA-sequencing (**Figure 5A**). With or without stimulation with 293T-gp120 cells, duoCAR-$T_{HCW9206}$ cells exhibited distinct transcriptional differences as compared to duoCAR-$T_{\alpha CD3/28}$ cells **(Figures S5)**. In the comparison of duoCAR-$T_{HCW9206}$ and duoCAR-$T_{\alpha CD3/28}$ cells with or without stimulation with gp120, we identified 311 unique differentially expressed genes (DEGs) in the absence of gp120-activation, 172 DEGs after gp120-activation, and 128 shared DEGs (**Figure 5B**). These results indicate that the largest transcriptional differences between duoCAR-$T_{HCW9206}$ and duoCAR-$T_{\alpha CD3/28}$ cells are observed in unactivated CAR-T cells; however, upon activation, their transcriptional profiles converge with lower amounts of DEGs, indicating an overlapping response to CAR stimulation by gp120. Specifically, we found that unactivated CAR-$T_{HCW9206}$ cells displayed an upregulation of cytokine-signaling and JAK/STAT signaling-associated gene transcripts as compared to unactivated CAR-$T_{\alpha CD3/28}$ cells, including *STAT3*, *IL15RA*, *IL-2RA*, *IL6R*, *SOCS1*, *SOCS2*, *SOCS3*, *FOS*, *JUN* (**Figures S6A, Figure S7 and S8**), as well as pro-inflammatory cytokines such as *TNF* and *IFNG* (**Figure S5B**).

DEGs identified for duoCAR-$T_{\alpha CD3/28}$ and duoCAR-$T_{HCW9206}$ cells were predicted by Ingenuity Pathway Analysis (IPA) to be associated with T-cell development and activation, JAK/STAT signaling, or T-cell migration and are shown in heat maps and pathway or gene set analyses (**Figures 5C, 5D, S6, S7, S8, and S9**). Specifically, IPA and pre-ranked gene set

enrichment analysis (GSEA) indicated strong upregulation of STAT3 (**Figure S7A**) and STAT5 (**Figure S7B**) signaling pathways in the comparison of unactivated duoCAR-$T_{HCW9206}$ and duoCAR-$T_{\alpha CD3/28}$ cells. We determined that duoCAR-$T_{HCW9206}$ cells compared to duoCAR-$T_{\alpha CD3/28}$, either unactivated (**Figure 5C and S6**) or activated (**Figure 5D and S9**) by 293T-gp120 cells, displayed significant (padj ≤ 0.05) upregulation of genes associated with cell migration (*CXCR4*), survival (*BCL2*), and T_{SCM} phenotype (*SMAD7, KLF2, IL7R*) (*25, 39-42*). Additionally, both unactivated and activated duoCAR-$T_{HCW9206}$ also demonstrated T-cell effector-like gene signatures as identified through IPA, including expression of *PRF1*, *NOTCH1*, *FAS*, *PRDM1,* and *ICOS* (**Figure 5C and 5D**). IPA analysis comparing the transcriptomes of unactivated CAR-$T_{HCW9206}$ cells and CAR-$T_{\alpha CD3/28}$ cells identified enrichment in CAR-$T_{HCW9206}$ for expression of genes associated with several pathways, including "Cell viability," "Cell survival," "Cell movement," and "Stimulation of T-lymphocytes" in the CAR-$T_{HCW9206}$ cells (**Figure 5E**). The enrichment for expression of genes involved in cell viability and survival pathways in CAR-$T_{HCW9206}$ cells, compared to CAR-$T_{\alpha CD3/28}$ cells, indicates an increased fraction of CAR-$T_{HCW9206}$ cells representing long-lived early-memory T_{SCM} cells. Additionally, comparing the transcriptomes of activated CAR-$T_{HCW9206}$ cells and CAR-$T_{\alpha CD3/28}$ cells revealed increased expression of genes in the CAR-$T_{HCW9206}$ cells related to effector function pathways, including "Cytotoxicity" and "Internalization of cells," as well as migratory pathways such as "Extravasation of cells." (**Figure S9C**). These results indicate that the transcriptome of CAR-$T_{HCW9206}$ cells, compared to that of CAR-$T_{\alpha CD3/28}$ cells, is enriched for cells with a pro-survival, T_{SCM}-like transcriptome while retaining a population with a robust effector T-cell transcriptome.

CD19-CAR-T$_{HCW9206}$ cells display increased in vivo functional persistence compared to CAR-T$_{\alpha CD3/28}$ in NSG mice rechallenged with NALM-6 leukemia cells

We examined whether enrichment of the CD19-CAR-T$_{HCW9206}$ cells for the T$_{SCM}$ phenotype, compared to the CD19-CAR-T$_{\alpha CD3/28}$ cells, increased their in vivo functional persistence by evaluating their ability to eliminate an initial challenge and subsequent rechallenge with NALM-6 leukemia cells expressing a luciferase reporter gene (NALM-6-Luc cells) injected into *Prkdc^{scid} RhRHIL-2rg^{tm1Wjl}/SzJ* (NSG) mice (**Figure 6A**). One day after NSG mice were intravenously engrafted with NALM-6-Luc cells (0.5 x 10^6 cells/mouse), the mice were intravenously injected with CD19 CAR-T$_{HCW9206}$ cells or CD19 CAR-T$_{\alpha CD3/28}$ cells (8:1 E:T ratio). Human IL-7, IL-15SA, and IL-21 to support the engrafted human T cells in the mice were provided by biweekly injections with HCW9206 (3mg/kg) (*43, 44*). Preliminary studies indicated that CAR-T cell function and persistence were enhanced in mice injected with HCW9206 compared to mice not treated with HCW9206 (**Figure S10A and S10B**). Interestingly, even in mice not treated with cytokines, we observed a trend of enhanced CD19 CAR-T$_{HCW9206}$ survival and delayed NALM-6-Luc cell expansion compared to CD19-CAR-T$_{\alpha CD3/28}$ cell-treated mice (**Figure S10C and S10D**). The population of NALM-6-Luc cells in mice was quantified weekly via bioluminescence imaging (BLI) (**Figure 6B**). Rapid expansion and systemic dissemination of NALM-6-Luc cells were observed 20 days after they were injected into mice that were either untreated or treated with untransduced T cells, either activated by αCD3/28 or treated with HCW9206 before engraftment. In contrast, we observed almost total inhibition of NALM-6-Luc cell growth in all the mice treated with CD19-CAR-T$_{HCW9206}$ cells or CD19-CAR-T$_{\alpha CD3/28}$ cells. To evaluate the persistence of functional CD19-CAR-T$_{HCW9206}$ cells or CD19-CAR-T$_{\alpha CD3/28}$ cells in these mice three weeks after the initial CD19-CAR-T cell injection,

we rechallenged them with a second injection of NALM-6-Luc cells (0.5 x 10^6). Evaluation of the mice by BLI demonstrated that while NALM-6-Luc cell dissemination was observed in 5 of 6 mice injected with CD19-CAR-$T_{\alpha CD3/28}$ cells, no NALM-6-Luc cell dissemination was detected in any of the 5 mice infused with CD19-CAR-$T_{HCW9206}$ cells (**Figure 6B**). This was confirmed by a significantly ($p = 0.0321$) reduced total photon flux measured in the mice treated with CD19-CAR-$T_{HCW9206}$ cells compared to mice treated with CAR-$T_{\alpha CD3/28}$ cells (**Figure 6C**). The potent suppression of NALM-6-Luc cell expansion after rechallenge in the mice treated with CD19-CAR-$T_{HCW9206}$ cells was associated with a significant increase in the number of circulating CD19-CAR-$T_{HCW9206}$ cells at 8 days ($p = 0.0053$) and 16 days ($p = 0.0008$) compared to barely detectable levels of circulating CD19-CAR-$T_{\alpha CD3/28}$ cells in the CD19-CAR-$T_{\alpha CD3/28}$ cell-treated mice (**Figure 6D**). This was paralleled by the consistently higher population of CD19-CAR-T cells with a T_{SCM} phenotype in the peripheral blood of mice injected with CD19-CAR-$T_{HCW9206}$ cells compared to mice injected with CD19-CAR-$T_{\alpha CD3/28}$ cells (**Figures 6E and 6F**). Specifically, 15 days after infusion, the fraction of CD19-CAR-T cells with a T_{SCM} phenotype in the peripheral blood of mice injected with CAR-$T_{HCW9206}$ cells (46.4% ± 25.9%) was almost 20-fold greater than the T_{SCM} population in the mice injected with CD19-CAR-$T_{\alpha CD3/28}$ cells (2.5% ± 5.6%); this likely contributes to the more persistent in vivo functional activity of CAR-$T_{HCW9206}$ cells compared to mice injected with CD19-CAR-$T_{\alpha CD3/28}$ cells. Furthermore, over 6 weeks after injection of the CD19-CAR-T cells and 3 weeks after rechallenging with NALM-6-Luc cells, we detected few CAR-T cells in the spleens (**Figure 6G**) and bone marrow (**Figure 6H**) of mice injected with CD19-CAR-$T_{\alpha CD3/28}$ cells. In contrast, we detected discrete populations of CD19-CAR-T cells in the spleens (**Figure 6G**) and bone marrows (**Figure 6H**) of all the mice injected with CD19-CAR-$T_{HCW9206}$ cells, which were significantly higher ($p = 0.0014$ and $p = 0.0098$,

respectively) than CD19-CAR-$T_{\alpha CD3/28}$ injected mice. Taken together, these data demonstrate that the CD19-CAR-$T_{HCW9206}$ cells exhibit robust engraftment, with significantly higher populations of CAR-T_{SCM} cells. This population is associated with enhanced persistence and a greater capacity to mount a protective proliferative response in vivo, as indicated by the effective suppression of tumor cell expansion after rechallenging with $CD19^+$ NALM-6-Luc cells by CD19-CAR-$T_{HCW9206}$ cells compared to CD19-CAR-$T_{\alpha CD3/28}$ cells.

Anti-HIV duoCAR-$T_{HCW9206}$ displays potent cytotoxic function in an HIV-1 PBMC humanized mouse model

We compared the capacity of duoCAR-$T_{HCW9206}$ cells and duoCAR-$T_{\alpha CD3/28}$ cells to suppress HIV infection using a humanized NSG mouse model of HIV-1 infection (hu-spl-PBMC-NSG) we had previously developed to establish the capacity of intravenously injected anti-HIV duoCAR-T cells to migrate into the spleen to suppress HIV infection (*17*). As outlined in the experimental protocol (**Figure 7A**), after NSG mice were intrasplenically injected with syngeneic PBMCs infected with $HIV\text{-}1_{JRCSF}$ (15×10^6 cells/mouse), they were either untreated, treated with controls of untransduced αCD3/CD28-activated T cells or HCW9206-treated T cells, or with duoCAR-$T_{HCW9206}$ cells or duoCAR-$T_{\alpha CD3/28}$ cells (15×10^6 cells/mouse). The mice were sacrificed after 17-18 days, and duoCAR-T cells, human lymphocytes, and the level of HIV infection in the spleens were quantified. While equivalent numbers of duoCAR-T cells were detected in the spleens of mice injected either with duoCAR-$T_{HCW9206}$ cells or duoCAR-$T_{\alpha CD3/28}$ cells (**Figure 7B**), the spleens of mice injected with duoCAR-$T_{HCW9206}$ cells displayed significantly greater ($p = 0.0173$) suppression of the number of HIV-infected cells (92.4%) compared to mice injected with duoCAR-$T_{\alpha CD3/28}$ cells (49.7%) as evaluated through an unpaired

nonparametric student's t-test (**Figure 7C**). We also observed an increased population of human $CD4^+$ T cells in the spleens of duoCAR-$T_{HCW9206}$ cell-injected mice compared to duoCAR-$T_{\alpha CD3/28}$ cell-injected mice (**Figure 7D**), likely reflecting an inverse correlation between the level of HIV infection in the mouse spleens and HIV-mediated $CD4^+$ T cell depletion. Together, this data indicates that duoCAR-$T_{HCW9206}$ cells display more potent in vivo anti-HIV activity than duoCAR-$T_{\alpha CD3/28}$ cells, possibly due to the enrichment of the T_{SCM} phenotype in the engrafted duoCAR-$T_{HCW9206}$ cells, which may provide a continuing source of new duoCAR-T_{EM} and effector cells that enable increased suppression of HIV infection.

Anti-HIV duoCAR-$T_{HCW9206}$ with potent effector function can be generated from PLWH

The goal of duoCAR-T cell treatment is to provide a persistent immune response capable of mediating sustained remission to PLWH. Consequently, we evaluated whether HCW9206 treatment of PLWH T cells also generated duoCAR-T cells enriched with a T_{SCM} phenotype, which should display the more persistent functional activity required to provide the sustained suppression of recurrent HIV infection, which would otherwise occur after the cessation of ART. As observed for people living without HIV (PLWoH) donors, HCW9206 treatment enabled equivalent transduction efficiency with the duoCAR-T LV of T cells from PLWH compared to αCD3/28 activation (**Figure 8A**). Furthermore, the fraction of $CD8^+$ duoCAR-T cells generated by HCW9206 treatment which were phenotypically T_{SCM} ($CD45RO^-CCR7^+CD95^+$) was ~15-fold greater (48.2% ± 18.0%) than the fraction of duoCAR-T cells that were T_{SCM} (3.2% ± 3.7%) produced by αCD3/28 activation as demonstrated by CD45RO vs. CCR7 expression in contour plots and CD95 and CD27 in histogram plots (**Figure 8B and 8C**). We evaluated the capacity of the duoCAR-$T_{HCW9206}$ cells compared to the duoCAR-$T_{\alpha CD3/28}$ cells from PLWH donors to

suppress HIV infection using an in vitro HIV-1 suppression assay as previously described (*17*). In brief, we superinfected CD8-depleted PBMCs derived from PLWH donors with the HIV-1-LucR IMC expressing the BaL envelope and 2 days later added autologous duoCAR-$T_{HCW9206}$ cells or duoCAR-$T_{\alpha CD3/28}$ cells at a 1:1 E:T ratio. As compared to HIV-infected CD8-depleted PBMCs alone and CD8-depleted PBMCs treated with UTD control T-cells, both duoCAR-$T_{HCW9206}$ cells and duoCAR-$T_{\alpha CD3/28}$ suppressed HIV-1 infection equivalently by >75% as shown in a representative experiment (**Figure 8D**) and combined data for 3 PLWH donors (**Figure 8E**). Thus, HCW9206 treatment of T cells from PLWH generates duoCAR-T cells composed of a highly enriched T_{SCM} population, which supports long-term persistence and functional activity in vivo, along with a T_{EM} population capable of providing immediate and potent HIV-1 suppression.

Discussion

Despite the capacity of ART to suppress HIV replication below the level of detection, sustained remission for PLWH after the cessation of ART is prevented by the persistence of the HIV viral reservoir capable of reintroducing systemic HIV (*11*). One strategy to achieve a functional cure for HIV is to augment the immune system of PLWH by introducing persistent, circulating immune cells with the capacity to recognize highly conserved HIV antigens (*13*). These cells should be resistant to HIV infection, able to overcome viral immune escape, and capable of migrating to sites of latent HIV infection to enable them to persist and quickly eliminate HIV-infected cells after reactivation to prevent recurrence of systemic infection. For this purpose, we developed and validated the potent anti-HIV activity of bispecific duoCAR-T cells (*16*). The duoCAR-T cells target two highly conserved epitopes of the HIV-1 envelope

glycoprotein, gp120, are highly resistant to HIV infection and migrate to active infection sites to effectively suppress HIV-1 infection in vivo in a hu-spl-PBMC-NSG mouse model (*16, 17*). However, the long-term efficacy of current CAR-T cell immunotherapy is limited by the loss of their functional activity over time after infusion into patients, particularly if their maturational state predominantly consists of terminally differentiated effector cells, which upregulate the expression of exhaustion markers and are associated with poor in vivo engraftment and anti-tumor activity (*24, 45*). In contrast, T cells comprising early memory T-cell phenotypes exhibit superior engraftment and better clinical outcomes after adoptive transfer compared to T cells derived from more differentiated memory precursors (*46*). One reason for the reduced persistence of infused CAR-T cells may be the use of strong CD3 and CD28 activation to enable transduction with LV encoding the CAR, which has the unintended consequence of driving rapid T cell differentiation and the production of suboptimal CAR-T cell products (*23, 47-50*). To address this, alternative strategies that do not involve CD3 and CD28 stimulation have been evaluated, which deliver sufficient activation to enable LV transduction and the generation of CAR-T cells, but induce a decreased level of T cell differentiation. One strategy replaced TCR-activation with IL-7 treatment. IL-7 increases the expression of the anti-apoptotic molecule BCL2 and induces G0 to G1 cell-cycle progression, enabling lentiviral transduction without driving T-cell differentiation (*36*). In the absence of CD3 activation, IL-7 treatment enabled transduction by LV to create TCR-modified T cells or CD19 CAR-T cells enriched in a T_{SCM} phenotype, which demonstrated improved tumor control in in vivo melanoma and lymphoma xenograft models compared to αCD3/28-stimulated cells (*21, 36*). However, these studies could not confirm the corresponding persistence of the circulating IL-7-stimulated engineered T cells. Similarly, previous studies have also shown that IL-7 and IL-15 better preserve the T_{SCM}

phenotype (*51, 52*). One study used isolated naïve T cells activated with αCD3/28 and cultured with IL-7 and IL-15 to generate CD19 CAR-T cells enriched in the T_{SCM} subset (*27*). Although these CAR-T_{SCM} cells displayed enhanced tumor suppression and corresponding CAR-T persistence, they were less cytotoxic compared to more differentiated CAR-T cell subsets (*27*). In the current study, we build on this prior research by incorporating IL-21 alongside IL-7 and IL-15SA delivered by a single scaffold protein to support the expansion of T cells with potent effector function while maintaining early memory phenotypes, including T_{CM} and T_{SCM} subsets (*51, 53, 54*). Previous reports have shown that IL-21 is crucial for the development and maintenance of early memory CD8 T cells (*55*), and it explicitly enhances survival and proliferation when combined with IL-7 or IL-15, benefiting both memory and naïve-like CAR-T cells (*56*). To the best of our knowledge, we are the first study to demonstrate the use of a novel tripartite cytokine scaffold for generating T_{SCM}-enriched, polyfunctional CAR-T cells. Notably, this study is also the first to utilize only cytokine-based activation signals for generating HIV-specific CAR-T cells. This advances HIV immunotherapy by introducing a new strategy that can produce a functionally persistent product, thereby extending the lifespan of anti-HIV CAR-T therapy in PLWH and potentially enabling a functional cure.

To deliver IL-7, IL-15SA, and IL-21 using a single agent, we developed HCW9206, a novel soluble tissue-factor fusion molecule that links IL-7, IL-15SA, and IL-21 to activate and expand memory-like NK cells (*32*). This scaffold is based on the IL-15 superagonist, N-803, and uses the corresponding IL-15/IL-15RaSu domains (*57*). However, HCW9206 builds on N-803 by additionally linking IL-7 and IL-21 cytokine domains, all joined by a tissue factor-based scaffold. This design simplifies the delivery of three synergistic cytokines in a single treatment and allows each cell interacting with the scaffold to engage all three cytokines simultaneously.

Here, we demonstrate for the first time that multi-cytokine scaffold treatment with HCW9206, without additional CD3 activation, enables the efficient production of both HIV- and CD19-specific CAR-T cells that are highly enriched for a T_{SCM} cell phenotype. Importantly, HCW9206 treatment also generates sufficient CAR-T effector cells that can elicit an immediate cytotoxic response, effectively suppress HIV infection and eliminate $CD19^+$ tumor cells. These results indicate that HCW9206 treatment provides benefits over standard αCD3/28 activation, as it generates both HIV-specific duoCAR-T cells (*16, 17*) and CD19-specific CAR-T cells enriched in CAR-T_{SCM}. These cells display potent in vivo suppression of HIV infection and leukemic cell growth, along with enhanced functional persistence (**Figures 6 and 7**).

We demonstrated that HCW9206-generated CAR-T cells, highly enriched in T_{SCM} cells, display a shift to a more differentiated memory and effector phenotype distribution after co-culture with their cognate antigen, either HIV gp120 or CD19, which indicated that the HCW9206-generated CAR-T cells were capable of both proliferating as well as expanding more differentiated T-memory cell progeny, both of which are critical for optimal effector responses (**Figures 2F and 3F**). Previous studies that generated CAR-T_{SCM} cells by pre-purifying T_{SCM} cells before CAR LV transduction produced CAR-T cells that were less cytotoxic than conventional αCD3/28-generated CAR-T cells (*27*). In contrast, we demonstrate, both in vitro and in vivo, that HCW9206-generated HIV-specific duoCAR-T cells are markedly enriched for the T_{SCM} phenotype, while also exhibiting cytotoxic function equivalent to that of CAR-$T_{\alpha CD3/28}$ cells (**Figure 4**). This is most likely due to the support of effector functions via combined IL-7 and IL-21 cytokine signals delivered through HCW9206, which have previously been shown to synergistically promote the expansion of cytotoxic T cells and the production of inflammatory cytokines (*48*). However, a potential challenge of the significant increase in inflammatory

cytokine production by duoCAR-$T_{HCW9206}$ cells compared to duoCAR-$T_{\alpha CD3/28}$ is the risk of inducing inflammatory cytokine release. Therefore, an important future direction of this study is the further evaluation of cytokine release syndrome in our humanized mouse models. An advantage of generating CAR-T cells using HCW9206 treatment compared to combinations of these, or other cytokines is that it utilizes a single biologic to leverage the independent and synergistic effects of three cytokines, IL-7, IL-15SA, and IL-21, simplifying dosing and regulatory approval for translation into clinical use. Taken together, these results indicate that CAR-T cell production using HCW9206 synergizes the effects of IL-7, IL-15SA and IL-21 to promote the generation of a CAR-T cell product with a diverse mix of T cell subsets which exhibit a combination of T_{SCM} self-renewal capacity and enhanced T cell effector function, likely from the T_{EM} population, indicating that CAR-$T_{HCW9206}$ may be a more effective and long-lasting CAR-T cell immunotherapy than conventional CAR-$T_{\alpha CD3/28}$.

RNA sequencing analysis of the transcriptome of HIV-specific duoCAR-T cells generated by IL-7, IL-15SA, and IL-21 treatment delivered by HCW9206, compared to αCD3/αCD28 activation, identified multiple uniquely expressed genes, including those associated with increased migratory and pro-survival pathways (**Figure 5**) (*25, 58*). Importantly, antigen stimulation of duoCAR-$T_{HCW9206}$ cells significantly upregulated the expression of *SATB1* (special AT-rich sequence-binding protein 1), a gene previously reported to be a key determinant in lineage commitment through chromatin reorganization. Specifically, *SATB1* has been shown to be a key regulator of $CD8^+$ T-cell quiescence and stemness (*59-61*), as well as promoting early effector cell expansion and differentiation to support both effector responses and long-term T-cell persistence (*61*). The transcriptome of antigen-stimulated duoCAR-$T_{HCW9206}$ compared to duoCAR-$T_{\alpha CD3/28}$ also displayed increased expression of *IL-10, IL-6,* and *STAT3,* which have

been previously reported to support CAR-T_{SCM} maintenance and are associated with CAR-T cell longevity in patients (*24, 31*). IPA analysis of the transcriptomes of resting duoCAR-$T_{HCW9206}$ cells compared to resting duoCAR-$T_{\alpha CD3/28}$ cells identified enrichment in DEGs associated with pathways including "Cell viability" and "Cell survival" (**Figure 5E**). The enrichment of genes involved in these pathways indicates the markedly increased population of long-lived, self-renewing early memory T-cell populations in the CAR-$T_{HCW9206}$ cell product compared to the CAR-$T_{\alpha CD3/28}$ cell product. Consistent with our in vitro studies, we also found that the transcriptome of antigen-stimulated duoCAR-$T_{HCW9206}$ cells showed enrichment in gene expression in pathways associated with "Cytotoxicity" and "Internalization of cells" as well as "Migratory pathways" compared to the transcriptome of antigen-stimulated duoCAR-$T_{\alpha CD3/28}$ (**Figure S9C**). These results suggest that duoCAR-$T_{HCW9206}$ cells are enriched in both a T_{SCM} phenotype, as indicated by pro-survival and T_{SCM}-like gene signatures, as well as more differentiated effector-like phenotypes, likely contributing to the potent HIV suppression observed both in vitro and in vivo.

In a humanized mouse model of HIV infection, we demonstrated that while both intravenously injected CAR-T cell types could localize to the site of HIV infection in the mouse spleen at comparable levels, anti-HIV duoCAR-$T_{HCW9206}$ cells demonstrated superior suppression of viremia compared to duoCAR-$T_{\alpha CD3/28}$ cells (**Figure 7**). Specifically, we demonstrated that in the mouse spleens injected with HIV-infected human PBMCs, the duoCAR-$T_{HCW9206}$ (92.4%) cells showed significantly increased suppression ($p = 0.0173$) of HIV infection compared to duoCAR-$T_{\alpha CD3/28}$ cells (49.7%). This indicates that, following migration to the spleen, the duoCAR-$T_{HCW9206}$ cells exhibited superior anti-HIV cytotoxic activity compared to duoCAR-$T_{\alpha CD3/28}$ cells. This enhanced activity may be a consequence of the increased population of T_{SCM}

519 cells in the engrafted duoCAR-$T_{HCW9206}$ cells, which may act as a renewable source of potent
520 effector cells to better control HIV infection. However, this study does not assess long-term anti-
521 HIV duoCAR-T efficacy against reactivated HIV-infected cells from latent HIV reservoirs.
522 Therefore, pairing our anti-HIV duoCAR-$T_{HCW9206}$ cells with a latency-reversing agent (LRA)
523 may be critical to achieving a functional cure for HIV. Previous studies have shown that an IL-15
524 superagonist such as N-803, with a similar structure to the IL-15SA component of the HCW9206
525 construct, can function independently as an LRA and display both latency reversal and successful
526 effector cell recruitment in vivo (*62-66*). Thus, an important future direction of this project is to
527 evaluate HCW9206 as an LRA to be paired with treatment with anti-HIV duoCAR-$T_{HCW9206}$
528 cells.

529 Using an NSG-humanized mouse model, we observed that CD19-CAR-$T_{HCW9206}$ cells,
530 but not CD19-CAR-$T_{\alpha CD3/28}$ cells, mounted a recall response to a second $CD19^+$ NALM-6
531 leukemia challenge, effectively preventing tumor dissemination. This response was associated
532 with a corresponding marked increase in CD19-CAR-T cell expansion in the blood, spleen, and
533 bone marrow of CD19-CAR-$T_{HCW9206}$ cell-treated mice compared to those treated with CD19-
534 CAR-$T_{\alpha CD3/28}$ cells (**Figure 6**). This correlated with the maintenance of circulating CD19-CAR-
535 T_{SCM} cells we observed 44 days after the mice were injected with CD19-CAR-$T_{HCW9206}$ cells, but
536 not with CD19-CAR-$T_{\alpha CD3/28}$ cells (**Figure 6E and 6F**). T_{SCM} cell enrichment in CAR-T cells
537 stimulated with HCW9206 represents a novel strategy for generating CAR-T cells, potentially
538 providing treated patients with more prolonged and effective protection against cancer relapses.

539 Taken together, these data demonstrate that treating T cells with a combination of IL-7,
540 IL-15SA, and IL-21 cytokines delivered by a single biologic, HCW9206, can quickly and
541 effectively produce HIV- and CD19-specific CAR-T cells that are highly enriched for the T_{SCM}

memory phenotype, as well as effector T cells capable of maintaining suppression of HIV and leukemic cell proliferation. Therefore, generating CAR-T cells through HCW9206 treatment could provide a new, improved, and highly scalable method for generating CAR-T cells to treat patients with cancer and infectious diseases and replace standard CAR-T cell production using αCD3/αCD28 activation. This has widespread implications for the generation of more robust CAR-T cell-based immunotherapies to improve CAR-T cell functional persistence and efficacy for the treatment of HIV and cancer.

Materials and Methods

Experimental Design

This study aims to characterize an alternative method for T-cell activation that enables CAR lentiviral transduction, generating a longer-lasting, early memory T_{SCM}-enriched CAR-T phenotype with increased potency and longevity. We hypothesized that stimulating T-cells with the cytokine scaffold HCW9206, which links IL-7, an IL-15/IL-15Rα sushi domain complex, and IL-21, would generate CD19- and HIV-specific CAR-T cells with an enriched T_{SCM} CAR-T cell memory phenotype, thereby increasing their sustained capacity to eliminate $CD19^+$ tumors and HIV-infected cells. In our study, we evaluated HCW9206-generated CD19- and HIV-specific CAR-T cells for their memory phenotype, cytotoxic function, and cytokine production. We also conducted comprehensive analyses to assess their stem-like properties, including proliferation and progeny generation assays. Additionally, we conducted an in vitro HIV-1 challenge using Renilla luciferase-expressing replication-competent infectious molecular clones of HIV-1 that express different HIV-1 clade B-derived Env genes (BaL-LucR and JRCSF-LucR) to compare HIV-1 suppression between anti-HIV duoCAR-$T_{\alpha CD3/28}$ and duoCAR-$T_{HCW9206}$ cells. The in vitro studies were conducted in at least three independent donors, who were either PLWoH or PLWH. The persistence of CD19-CAR-$T_{HCW9206}$ cells was further interrogated in a long-term in vivo NSG mouse model of $CD19^+$ acute lymphoblastic leukemia (ALL). NSG mice were challenged with $CD19^+$ Firefly luciferase-expressing NALM-6-Luc cells one day before treatment with CD19-CAR-T cells and re-challenged with NALM-6-Luc tumor 21 days into the study to evaluate the persistence of CD19-CAR-$T_{HCW9206}$ cells compared to CD19-CAR-$T_{\alpha CD3/28}$ cells. The study tracked tumor burden using IVIS bioluminescent imaging and circulating CAR-T cell levels through regular peripheral blood sampling. At the end of the study, the mice were

sacrificed, and their spleens and bone marrow were harvested for flow cytometric analysis of CAR-T populations. We also investigated the in vivo efficacy of anti-HIV duoCAR-$T_{HCW9206}$ cells using a humanized NSG mouse model of HIV infection wherein HIV-infected PBMCs are intrasplenically engrafted into the mice (hu-spl-PBMC-NSG) before intravenous duoCAR-T delivery. At the study endpoint, the mice were sacrificed for the following endpoint analysis: (1) flow cytometry of processed murine spleen for $CD4^+$ T-cell depletion, (2) detection of duoCAR-T cells by analyzing total splenocyte-associated duoCAR DNA copies by ddPCR of mouse spleens, and (3) HIV-1 suppression by analyzing total splenocyte-associated HIV-1 DNA by ddPCR. In all in vivo studies, at least four mice per treatment cohort were selected for statistical power, with an equal distribution of male and female mice.

Mice

For all in vivo experiments, >3-month-old female and male *NOD.Cg-Prkdc^{scid} RhRHIL-2rg^{tm1Wjl}/SzJ* (NSG) mice were used. NSG mice were obtained from the Jackson Laboratory (RRID: IMSR_JAX:005557) and bred at Albert Einstein College of Medicine, where they were housed in a BSL-2+ animal facility under a 12-hour light/dark cycle.

Cell lines

Human NALM-6 (acute lymphoblastic leukemia) and Raji cells (B cell Burkitt's lymphoma) were obtained from X. Zang (Albert Einstein College of Medicine, Bronx, NY). Human embryonic kidney (HEK) 293T cells (human kidney epithelium) and $TCR\beta^{-/-}$ Jurkat/MA (JurMA) cells, which are a derivative of the T-cell leukemia $CD8^+$ Jurkat J.RT3-T3.5 cells expressing an NFAT promoter, were obtained as a gift from A. Follenzi and E. Hooijberg (VU University Medical Center, Amsterdam, The Netherlands), respectively (*67*). Cell lines were grown in Iscove's Modified Dulbecco's Modified Eagle's Medium DMEM (IMDM) (Corning,

Ref# 10-016-CV) or RPMI 1640 medium (Corning, Ref# 10-040-CV) supplemented with 10% fetal bovine serum (FBS), 1X GlutaMAX (Gibco, Ref# 35050-061), 1X Penicillin-Streptomycin Solution (Corning, Ref# 30-002-CI), and 100 mM HEPES buffer and cultured in a humidified incubator at 37°C and 5% CO2.

Generation of firefly luciferase$^+$ NALM-6 cell line (NALM-6-Luc)

HEK293T cells were co-transfected with a Luciferase-tdTomato (-Luc) plasmid obtained from X. Zang (Albert Einstein College of Medicine) and three packaging plasmids (pCMV-VSV-G, pMDL - gag/pol, and REV) through calcium phosphate precipitation. Two days later, the LV supernatant was concentrated by ultracentrifugation at 20,000 x g for 2h and 15 minutes at 20ºC. NALM-6 cells were seeded at 2 x 10^5 cells/mL in a 6-well plate and transduced with the Luc-encoding LV in the presence of LentiBlast Premium Transduction Enhancer (2 µL/mL) (OZ Biosciences, Ref# LBPX500). Transduced cells were sorted for tdTomato (RFP) expression three times to ensure a pure NALM6-Luc population using a BD FACS Aria II cell sorter.

Construction and production of HCW9206 heterodimeric fusion protein

As previously described, the heterodimeric protein scaffold, HCW9206, developed and produced by HCW Biologics, is a complex of two fusion proteins linked by a human tissue factor (TF) scaffold (*32*), IL-7 linked to the N-terminus of the extracellular domain (aa1-219) of the TF and IL-21 linked to the N-terminus of the sushi domain of IL-15Rα (rhIL-15RαSu). Briefly, after CHO.K1 cells (ATCC, Ref# CCL-61) are transfected with the two different pMSGV-1-derived vectors, they express encoded fusion proteins, which form the HCW9206 protein complex through high-affinity interactions between the rhIL-15 and rhIL-15RaSu domains. HCW9206 was purified using immunoaffinity chromatography, and the bioactivity of

each cytokine domain was assessed using proliferation assays on IL-7 (2B8) (Sigma), IL-15 (CTLL-2) (ATCC, Ref# TIB-214), and IL-21 (B9) (Sigma, Ref# 12121201) dependent cell lines (*32*).

Construction of CAR lentiviral vectors

The anti-CD19 scFv (X. Zang; Albert Einstein College of Medicine, Bronx, NY) is linked to a human CD8α hinge and transmembrane domain, costimulatory molecules (CD28 and 4-1BB), and finally the intracellular domain of human CD3ζ. The entire anti-CD19 CAR sequence was subcloned into a lentiviral expression plasmid under the control of an SFFV promoter, followed by a self-cleaving T2A peptide sequence and an eGFP reporter sequence for CAR detection. The lentivirus expression plasmid was modified from the pCCLsin.PPT.SFFV.IRES.eGFP.Wpre plasmid obtained from A. Follenzi (*68*). The anti-HIV duoCAR expression vector (MND-ΔW) was generated as previously described (*17*). Briefly, the bicistronic anti-HIV duoCAR-encoding sequence (MND-ΔW) was generated wherein encoding sequences for each CAR domain (mD1.22 and m36.4) was subcloned in frame to encoding sequences for a CD8 ectodomain, CD8 transmembrane domain, 4-1BB costimulatory domain, and CD3ζ T-cell signaling domain. A P2A site was also placed downstream of the first CAR (mD1.22), followed by the second CAR domain (m36.4) with a corresponding CD3ζ signaling domain.

Lentiviral vector production of anti-HIV duoCAR and CD19 CARs

LV expressing either anti-HIV duoCAR or CD19 CAR transgenes was produced by transiently transfecting HEK293T cells. Using a 3-plasmid system, HEK293T cells were co-transfected with the CAR transfer plasmid (10μg), VSVG envelope (pMD2.g; 2.5μg), and a

packaging plasmid co-expressing gag, pol, and rev (psPAX; 7.5µg). psPAX and pMD2.g plasmids were obtained from C. Zhang (UT Southwestern Medical Center, Dallas, TX). Transfection was performed in >80% confluent HEK293T cells using JetPrime (Polyplus, Ref# 101000046) reagents following the manufacturer's instructions. After two days, the lentiviral particles were harvested from the supernatant by ultracentrifugation at 20,000 × g for 2 hours and 15 minutes at 20 °C. The pellet containing the lentiviral particles was resuspended, aliquoted, and stored at -80 °C. The infectious titer was calculated by limiting dilution titration in a human JurMA cell line, wherein the lentiviral titer is expressed as transduction units per milliliter (TU/mL).

Generation of CD19- and anti-HIV CAR-T cells through lentiviral transduction

PBMCs were obtained from donors recruited and leukapheresed through the Einstein-Rockefeller-CUNY Center for AIDS Research (ERC-CFAR), which includes PLWH and PLWoH. Highly purified $CD4^+$ and $CD8^+$ T cells were isolated from PBMCs as previously described (*16*) by immunomagnetic sorting using human anti-CD4 (Miltenyi Biotec, Ref# 130-045-101) and anti-CD8 (Miltenyi Biotec, Ref# 130-045-201) microbeads according to the manufacturer's protocol. T-cells were then activated with 1nM of recombinant human IL-7 (National Institutes of Health [NIH]), IL-15 (NIH), or IL-21 (R&D Systems, Cat# 219-IL-005) cytokines or 100nM of HCW9206 in supplemented IMDM media for 7-days before lentiviral transduction. Alternatively, T-cells were activated with αCD3(OKT3) (BioLegend, Ref# 317347) and αCD28 (BioLegend, Ref# 302943) antibodies at 100 ng/mL and 2 µg/mL, respectively, in the presence of IL-2 (100 U/mL; NCI-Frederick BRB Repository, NIH) for 3 days. The IMDM was supplemented with 10% FBS, 1X GlutaMAX, 1X Penicillin-Streptomycin Solution, and 100 mM HEPES buffer. After activation, T cells were transduced with αCD19-CAR or αHIV-

duoCAR LV in the presence of LentiBlast, as per the manufacturer's instructions. T cells were transduced at an MOI of 40-50 and spinfected at 2500 RPM (1139 x g) for 60 min, and the cell culture density was adjusted to a final concentration of 5 x 10^5 cells/mL. LV transduction efficiency was evaluated by flow cytometric staining 5-10 days post-transduction, as described below.

Flow cytometry of CAR-T cells

Approximately 5-10 x 10^5 cells untransduced or CAR-transduced primary T cells were washed with FACS buffer (1× PBS with added 5% FBS and 1 mg/mL sodium azide), incubated in human Fc blocking reagent (Miltenyi Biotec, Ref# 130-059-901) and/or mouse Fc blocking reagent (BD Biosciences, Ref# 553131) for 10 minutes at room temperature and then were stained interchangeably with the following conjugated antibodies for 20-30 minutes at 4°C: CD3-VioBlue (Miltenyi Biotec, Ref# 130-113-133), CD3-BUV395 (BD Bioscience, Ref# 563546), CD8-APC/Cy7 (BioLegend, Ref# 301016), CD8-PerCP/Cy5.5 (BioLegend, Ref# 344710), CD8-Pacific Blue (BioLegend, Ref# 301033), CD8-FITC (BioLegend, Ref #344703), CD4-PE (Miltenyi Biotec, Ref# 130-113-214), CD4-PE/Cy7 (BioLegend, Ref# 300512), CD4-FITC (BioLegend, Ref# 357405), CCR7-FITC (BioLegend, Ref# 353215), CCR7-BV711 (BioLegend, Ref# 353228), CCR7-APC (BioLegend, Ref# 353214), CD62L-BV650 (BioLegend, Ref# 304832), CD27-PE/Dazzle594 (BioLegend, Ref #356422), CD95-BV510 (BioLegend, Ref# 305640), CD45RA-PE/Cy7 (BioLegend, Ref# 304125), CD127-PerCP/Cy5.5 (BioLegend, Ref# 351321), CD45RO-APC/Cy7 (BioLegend, Ref# 304228), CD45RO-PE (BioLegend, Ref# 304206), NKG2A-PE (BioLegend, Ref# 375103), LAG3-PE (BioLegend, Ref# 369306), LAG3-PE/Cy7 (BioLegend, Ref# 369310), PD1-FITC (Invitrogen, Ref# 11-9969-42), PD1-Alexa Fluor 700 (BioLegend, Ref# 329952) or TIM3-BV650 (BioLegend, Ref#

345027). Additionally, for the detection of anti-HIV duoCAR, we used conjugated antibodies to an m36.4 idiotype, m36.4-FITC and/or m36.4-APC (Caring Cross, Gaithersburg, MD). The GFP reporter gene was used to detect transduction with the CD19 CAR LV. In some experiments, stained cells were fixed using 2% paraformaldehyde solution before analysis. All samples were analyzed using a Cytek Aurora flow cytometer, and data analysis was performed using FlowJo software. Cell counts are calculated based on flow cytometric gating using FlowJo software and accounting for the total staining well volume of 200 µL per sample.

Intracellular cytokine secretion evaluation

Donor-derived CD19-specific or anti-HIV duoCAR-T cells were plated in IMDM media at 2 x 10^6 cells/mL and cultured with target cells expressing cognate antigen, either $CD19^+$ NALM6 cells or HEK293T-gp120 cells (Caring Cross, Gaithersburg, MD), respectively, at a 1:1 E:T ratio for 16 hours in the presence of monensin (BioLegend, Ref# 420701) and brefeldin A (BioLegend, Ref# 420601) according to the manufacturer's instructions, to prevent secretion of intracellular cytokines. Each CAR-T cell analysis was set up in triplicate, and at the end of the time point, the cells were collected, washed with FACS buffer, and stained with LIVE/DEAD™ Fixable Viability Dye (Fisher Scientific, Ref# L34962) prior to incubation with human Fc block. Cells were incubated with surface staining antibodies for 30 minutes at 4°C: CD8-APC/Cy7, CD45RO-PE, CCR7-APC, m36.4-FITC (or GFP for CD19 CAR). Following incubation, cells were fixed using 2% paraformaldehyde and permeabilized using eBioscience™ Foxp3/Transcription Factor Staining Buffer Set (eBioscience, Ref# 00-5523-00) according to the manufacturer's protocol. Subsequently, the cells were incubated with the following intracellular antibodies for 1 hour at room temperature or at 4°C overnight: IL-2-PerCP/Cy5.5 (BioLegend, Ref# 500321), IFNγ-BV605 (BioLegend, Ref# 502536), TNFα-PE/Cy7 (BD Biosciences, Ref#

560678), TNFα-BV711 (BioLegend, Ref# 502939) or TCF1-Alexa Fluor 647 (BioLegend, Ref# 655203).

T cell proliferation and STAT5/STAT3 phosphorylation

For T cell proliferation assays, PBMCs derived from PLWoH were thawed and stained with Cell Trace Violet (2μM, CTV) (Invitrogen, Ref# C34557) for 20 minutes at 37℃. PBMCs were then stimulated with either anti-CD3/anti-CD28 in the presence of IL-2 (100U/mL) or HCW9206 (100nM). Seven days after stimulation, cells were stained for the level of CTV expression and analyzed by flow cytometry. Similarly, to assess STAT5 or STAT3 phosphorylation, PBMCs were thawed, and CD8 T cells were isolated as described above. Isolated T cells were plated overnight in a flat 96 well plate (2 x 10^6 cells/mL) in serum-free IMDM. Plated cells were either unstimulated or stimulated with 1nM IL-7, IL-15, IL-21, or 100nM HCW9206 and rested for 15-30 minutes at 37℃. paraformaldehyde solution (1.6%) was added to each well and incubated at room temperature for 10 min. Cells were washed with FACS buffer and centrifuged at 1300 RPM for 5 minutes. The supernatant was removed, and chilled methanol (100uL) was added to each well to permeabilize the cells for 30 minutes at 4℃. The cells were then washed with FACS buffer and resuspended in pSTAT5-Alexa Fluor 647 (BioLegend, Ref# 612599) or pSTAT3-FITC antibody (BioLegend, Ref# 651020). Cells were washed with FACS buffer before flow cytometric analysis.

In vitro anti-HIV duoCAR-T cell killing of HIV-1-infected donor cells

$CD4^+$ T-cells derived from HIV seronegative donors or PBMCs derived from HIV seropositive donors were cultured in supplemented IMDM media and activated with IL-2 (100 U/mL) and Phytohemagglutinin-L (PHA-L) (4ug/mL) (Roche, Ref# 11249738001) for 72 hours before infection with HIV-LucR-IMC as previously described (*16, 17*). For studies using PLWH

donors, $CD8^+$ T-cells were depleted from donors' PBMCs through immunomagnetic CD8 bead isolation before activation. Autologous activated CD4 T-cells or CD8-depleted PBMCs were washed, plated in a 96 U-bottom plate with 5 x 10^4 or 10 x 10^5 cells/well, respectively, and spinfected at 2500 RPM (1139 x g) for 90 minutes at room temperature with the indicated HIV-LucR IMC virus (~1 x 10^6 IU/mL). The HIV-LucR IMC used in this study were VRC01-sensitive HIV-1 Env strains JR-CSF and BaL (*69*). As previously described, the virus stocks were titered (IU/mL) on the TZM-bl reporter cell line (NIH AIDS Research and Reference Reagent Program [NIH ARRRP], Division of AIDS, NIAID, NIH, Ref # 8219) (*70*). Infection was established for 3 days before co-culture with autologous $CD8^+$ anti-HIV duoCAR-T cells or UTD control T-cells at the indicated E:T ratios. The co-cultures were incubated for an additional 3 days, after which the cells were lysed, and HIV-1 infection was quantified by measuring relative luciferase (LucR) using the Renilla Luciferase System (Promega, Ref# E2820) as previously described (*70*). The percentage of HIV-1 suppression was calculated as (1-CAR_{RLU}/HIV^+_{RLU} or UTD_{RLU}) x 100%.

Europium TDA (EuTDA) in vitro CD19 CAR-T cell killing assay

Cytotoxic activity of CD19-specific CAR-T cells was assessed using DELFIA EuTDA Cytotoxicity Reagents (PerkinElmer, Ref# AD0116) and $CD19^+$ NALM6 or Raji cells as target cells. Target cells were stained with BATDA reagent (1.3µL/1 x 10^6 cells) and incubated for 30 minutes at 37°C. Target cells were washed with media containing probenecid (2.5mM) to reduce the background signal. Target cells (1 x 10^5) were plated in a 96-well U-bottom plate and co-cultured with CD19 CAR-T cells or UTD control T-cells for 3 hours at 37°C at the indicated E:T ratios. After incubation, supernatant (20µL) was transferred to a microtiter plate, and Europium Solution (200µL/well) was added. After 15 minutes of incubation on a plate shaker at room

temperature, time-resolved fluorescence was quantified on a fluorescent plate reader equipped with DELFIA time-resolved fluorescence detection. The % target cell-specific lysis was calculated using the formula: % Specific Lysis = (Experimental Release – Spontaneous Release) / (Maximum Release – Spontaneous Release) x 100%.

Progeny generation assays and Inhibitory Receptor Assays

To assay CAR-T progeny generation in T_{SCM}-enriched CAR-$T_{HCW9206}$ cells, CAR-T cells were co-cultured with target cells expressing cognate antigen for 4 days. CD19-specific or HIV-specific duoCAR-T cells were phenotyped for memory markers using FACS analysis before co-culturing with NALM-6 or 293T-gp120 target cells, respectively, at a 2:1 E:T ratio for 4 days on a 24-well plate. After co-culture, cells were collected and phenotyped at the end time point using flow cytometric analysis. Similarly, the expression of inhibitory receptors was assayed in CAR-T cells either before or after 24 hours of co-culture with cognate antigen. Specifically, 293T-gp120 target cells (2×10^4) were plated in a 96-well U-bottom plate and co-cultured with HIV-specific duoCAR-T cells (1×10^5), respectively (5:1 E:T). One day after co-culture, the cells were collected and stained for CAR expression and inhibitory receptor expression (e.g. PD-1, TIM3, LAG3) and analyzed by flow cytometry.

RNA-sequencing: Library preparation

$CD8^+$ CAR-T cells generated following HCW9206 (100nM) or anti-CD3/28 activation with added IL-2 (100U/mL) were co-cultured for 16 hours with HEK293T (293T) or 293T-gp120 cells at a 5:1 E:T ratio in supplemented IMDM media. After 16-hours, cells were collected, washed with FACS buffer, and stained with αCD8-APC/Cy7 and the duoCAR detection antibody (m36.4-FITC). Additionally, cells were resuspended in a viability dye (DAPI)

(Sigma) before sorting the $CD8^+$ $m36.4^+$ duoCAR-T cells into RLT Plus lysis buffer using a BD FACSAria II cell sorter. RNA was purified using the micro-RNeasy Plus kit following the manufacturer's instructions (Qiagen, Ref# 74034). This protocol was repeated for each biological replicate. RNA sequencing was performed using Novogene's human mRNA sequencing pipeline, including RNA sample QC, RNA purification, mRNA library preparation (poly A enrichment), and the NovaSeq X Plus Series (PE150) sequencing platform.

RNA-sequencing: Read processing, alignment, and quantification

Quality control assessments of raw sequencing reads were performed using FastQC (version 0.11.9, Babraham Bioinformatics), validating data quality. Adapter sequences and low-quality bases were trimmed using Cutadapt (version 2.0) to ensure high-quality read retention. The processed reads were then mapped to the GRCh38human genome reference using the STAR aligner (version 2.4.2a) with default parameters. Following alignment, gene-level read quantification was conducted using featureCounts (version 1.5.0, from the Subread package), utilizing gene annotations from the ENSEMBL GTF file (release 110).

RNA-sequencing: Differential expression analysis

Gene expression differences were analyzed using DESeq2 (version 1.34.0) in R. To minimize noise from low-expressed genes, filtering was applied to remove genes where at least 80% of samples had fewer than 10 raw counts or where all samples exhibited zero expression. DESeq2 employs the Wald test to assess statistical significance, with multiple testing corrections performed via the Benjamini-Hochberg procedure. Genes with an adjusted p-value < 0.05 and an absolute log2 fold-change > 1.5 were classified as significantly differentially expressed. Regularized log-transformed (rlogTransformation) count data were used for principal component analysis (PCA) and hierarchical clustering-based heatmaps, allowing visualization of global

expression patterns across samples. For gene pathway analysis, Ingenuity Pathway Analysis (IPA; Qiagen) was utilized. DEGs for each comparison were uploaded for analysis, with filtering for observed relationships across all species and cell lines, excluding categories containing the terms “cancer” or “injury”. The top predicted gene functions were identified as functions with the lowest p-values, followed by the highest absolute value associated with z-score, with parameters of padj ≤ 0.05, $|\log2 \text{ (Fold Change)}| \geq 1$, $|\text{z-score}| \geq 2$. For the pre-ranked GSEA, 289 DEGs (adjusted $p < 0.05$) were ranked from the most significantly upregulated to the most significantly downregulated genes. Analysis of Hallmark gene sets was performed at 1,000 permutations, a minimum gene set size of 10 (filtering out 40 of 50 gene sets), and classic enrichment statistics.

In vivo intravenous NALM-6 leukemia tumor NSG mouse model

NSG mice were intravenously injected with NALM-6-Luc cells (5×10^5 cells) one day before engraftment with CD19 CAR-T cells or UTD control T-cells at an 8:1 E:T ratio and a 1:1 ratio of CD4:CD8 effector T-cells. Tumor-bearing mice were re-challenged with intravenously infused NALM-6-Luc cells (5×10^5 cells) 21 days after the initial tumor injection. All mice were sacrificed at a single endpoint (Day 44). Tumor burden was tracked via IVIS bioluminescent imaging over 44 days. At the end point, mice were sacrificed, and peripheral blood, spleen, and bone marrow were harvested for immune cell isolation and flow cytometric analysis.

In vivo hu-spl-PBMC-NSG mouse model of HIV-1 infection

We studied the in vivo efficacy of anti-HIV duoCAR-T cells using our previously described hu-spl-PBMC-NSG mouse model (*16, 17*). NSG mice were intrasplenically injected with HIV-infected PBMCs (15×10^6 cells), and then duoCAR-T cells were intravenously

delivered at a 1:1 E:T ratio, along with a 1:1 ratio of CD4:CD8 effector T cells. Mice were sacrificed at a single endpoint (Day 17-18). Spleens were harvested at the endpoint, and immune cells/splenocytes were isolated for further analyses, including quantification of total cell-associated HIV-DNA and duoCAR-DNA in total splenocytes by ddPCR, and T-cell analysis by flow cytometry.

Bioluminescent imaging

All studies using bioluminescent imaging were performed using the IVIS Spectrum in vivo Imaging System (PerkinElmer), and data analysis was completed using the Living Image software (version 3.0). All mice received an intraperitoneal injection of D-luciferin (150 µg/g mouse) (Gold Biotechnology, Ref# LUCNA) and were scanned at 15 minutes post-injection.

Immune cell isolation from mouse blood, spleen, and bone marrow

Bone marrow cells were harvested from mouse femurs, filtered through a 70µM strainer, washed, and centrifuged at 3500 RPM (1595 x g) for 10 minutes. The supernatant was removed, and cells were incubated with 1X RBC lysis buffer for 1.5 minutes at 4°C. In parallel, spleens were harvested from mice, disassociated, filtered through a 70µM strainer, washed, and centrifuged at 1300 RPM (592 x g) for 10 minutes. Cells were resuspended in 1X RBC lysis buffer and incubated for 5 minutes at 4°C. Peripheral blood (200µL/mouse) was collected from submandibular bleeding into anti-coagulant EDTA-coated collection tubes. Blood was strained through a 70µM strainer, washed, and resuspended in 1X RBC lysis buffer. All cells were washed and resuspended in FACS buffer before flow cytometric staining. Human T-cell counts from blood, bone marrow, and spleen were quantified via flow cytometric analysis using FlowJo software, with absolute cell numbers normalized to the total processed sample volume. Plasma

was isolated from peripheral blood via centrifugation of EDTA-coated collection tubes at 8000 RPM (3645 x g) for 8 minutes.

Detection of total cell-associated HIV DNA in mouse splenocytes by ddPCR

Total HIV DNA in the spleens of hu-spl-PBMC-NSG mice was detected by ddPCR using primers that target a region with the HIV-1 Gag gene that is not present in the CAR lentivirus itself, after following the manufacturer's instructions. DNA was isolated from whole spleens using the AllPrep DNA/RNA Kit (Qiagen, Ref# 80204). The DNA concentration was determined using a Nanodrop 2000 Spectrophotometer (ThermoFisher), and the copies of HIV-1 Gag DNA (25ng/µL) in the mouse spleens were quantified using PrimePCR Custom Assay HIV primer pairs/probe mixes (Bio-Rad, Hercules, California). Specifically, we used the HIV-Gag primer/probe mix sequences of the HIV-Gag3 region: forward primer (5'-TCAGCCCAGAAGTAATACCCATGT-3'), reverse primer (5'-CACTGTGTTTAGCATGGTGTTT-3'), and probe (5'-ATTATCAGAAGGAGCCACCCCACAAGA-3') with dye quencher (5' 6-FAM, 3' Iowa Black FQ). A splenic DNA sample (250 ng) was amplified using the primers/probes specific to HIV-1 Gag and each run included an HIV-negative human sample and a non-template control. ddPCR HIV-1 Gag sample results were quantified by QuantaSoft software and reported as copies/µL of DNA for each sample. All samples were then normalized to 25ng/µL of DNA. Results were displayed as total HIV-1 Gag copies/1 x 10^6 splenocytes. Statistical analysis was performed using one-way ANOVA between groups using GraphPad Prism with significance set at $p < 0.05$.

Study Approval

Written informed consent was obtained from PBMC donors under protocols approved by the Institutional Review Boards of the Albert Einstein College of Medicine and Rockefeller

University (protocol #2017-8116). Animal studies were conducted under a protocol approved by the Albert Einstein College of Medicine Institutional Animal Care and Use Committee (protocol #0001105) and were performed in accordance with the NIH Guide for the Care and Use of Laboratory Animals.

Statistical Analysis

All statistical analyses were performed using GraphPad Prism (version 9.5.1), with the statistical tests described in each figure legend. For all figures except Figure 5, which represents the RNA-sequencing dataset, data are presented as mean ± SEM from triplicate technical replicates, with statistical tests performed across biological replicates for a minimum of N = 3 donors. For RNA sequencing analyses, the data represent biological replicates from two independent donors. For all tests, the cutoff for statistical significance was a p-value of 0.05 and a padj value of 0.05 for RNA sequencing analyses.

References

1. M. Wang, J. Munoz, A. Goy, F. L. Locke, C. A. Jacobson, B. T. Hill, J. M. Timmerman, H. Holmes, S. Jaglowski, I. W. Flinn, P. A. McSweeney, D. B. Miklos, J. M. Pagel, M.-J. Kersten, N. Milpied, H. Fung, M. S. Topp, R. Houot, A. Beitinjaneh, W. Peng, L. Zheng, J. M. Rossi, R. K. Jain, A. V. Rao, P. M. Reagan, KTE-X19 CAR T-Cell Therapy in Relapsed or Refractory Mantle-Cell Lymphoma. *New England Journal of Medicine* **382**, 1331–1342 (2020).
2. F. L. Locke, A. Ghobadi, C. A. Jacobson, D. B. Miklos, L. J. Lekakis, O. O. Oluwole, Y. Lin, I. Braunschweig, B. T. Hill, J. M. Timmerman, A. Deol, P. M. Reagan, P. Stiff, I. W. Flinn, U. Farooq, A. Goy, P. A. McSweeney, J. Munoz, T. Siddiqi, J. C. Chavez, A. F. Herrera, N. L. Bartlett, J. S. Wiezorek, L. Navale, A. Xue, Y. Jiang, A. Bot, J. M. Rossi, J. J. Kim, W. Y. Go, S. S. Neelapu, Long-term safety and activity of axicabtagene ciloleucel in refractory large B-cell lymphoma (ZUMA-1): a single-arm, multicentre, phase 1-2 trial. *Lancet Oncol* **20**, 31–42 (2019).
3. E. Lugli, M. H. Dominguez, L. Gattinoni, P. K. Chattopadhyay, D. L. Bolton, K. Song, N. R. Klatt, J. M. Brenchley, M. Vaccari, E. Gostick, D. A. Price, T. A. Waldmann, N. P. Restifo, G. Franchini, M. Roederer, Superior T memory stem cell persistence supports long-lived T cell memory. *The Journal of Clinical Investigation* **123**, 594–599 (2013).
4. S. S. Neelapu, F. L. Locke, N. L. Bartlett, L. J. Lekakis, D. B. Miklos, C. A. Jacobson, I. Braunschweig, O. O. Oluwole, T. Siddiqi, Y. Lin, J. M. Timmerman, P. J. Stiff, J. W. Friedberg, I. W. Flinn, A. Goy, B. T. Hill, M. R. Smith, A. Deol, U. Farooq, P. McSweeney, J. Munoz, I. Avivi, J. E. Castro, J. R. Westin, J. C. Chavez, A. Ghobadi, K. V. Komanduri, R. Levy, E. D. Jacobsen, T. E. Witzig, P. Reagan, A. Bot, J. Rossi, L. Navale, Y. Jiang, J. Aycock, M. Elias, D. Chang, J. Wiezorek, W. Y. Go, Axicabtagene Ciloleucel CAR T-Cell Therapy in Refractory Large B-Cell Lymphoma. *N Engl J Med* **377**, 2531–2544 (2017).
5. S. J. Schuster, M. R. Bishop, C. S. Tam, E. K. Waller, P. Borchmann, J. P. McGuirk, U. Jäger, S. Jaglowski, C. Andreadis, J. R. Westin, I. Fleury, V. Bachanova, S. R. Foley, P. J. Ho, S. Mielke, J. M. Magenau, H. Holte, S. Pantano, L. B. Pacaud, R. Awasthi, J. Chu, Ö. Anak, G. Salles, R. T. Maziarz, Tisagenlecleucel in Adult Relapsed or Refractory Diffuse Large B-Cell Lymphoma. *N Engl J Med* **380**, 45–56 (2019).
6. J. S. Abramson, M. L. Palomba, L. I. Gordon, M. A. Lunning, M. Wang, J. Arnason, A. Mehta, E. Purev, D. G. Maloney, C. Andreadis, A. Sehgal, S. R. Solomon, N. Ghosh, T. M. Albertson, J. Garcia, A. Kostic, M. Mallaney, K. Ogasawara, K. Newhall, Y. Kim, D. Li, T. Siddiqi, Lisocabtagene maraleucel for patients with relapsed or refractory large B-cell lymphomas (TRANSCEND NHL 001): a multicentre seamless design study. *Lancet* **396**, 839–852 (2020).
7. J. G. Berdeja, D. Madduri, S. Z. Usmani, A. Jakubowiak, M. Agha, A. D. Cohen, A. K. Stewart, P. Hari, M. Htut, A. Lesokhin, A. Deol, N. C. Munshi, E. O'Donnell, D. Avigan, I. Singh, E. Zudaire, T.-M. Yeh, A. J. Allred, Y. Olyslager, A. Banerjee, C. C. Jackson, J. D. Goldberg, J. M. Schecter, W. Deraedt, S. H. Zhuang, J. Infante, D. Geng, X. Wu, M. J. Carrasco-Alfonso, M. Akram, F. Hossain, S. Rizvi, F. Fan, Y. Lin, T. Martin, S. Jagannath, Ciltacabtagene autoleucel, a B-cell maturation antigen-directed chimeric antigen receptor T-cell therapy in patients with relapsed or refractory multiple myeloma (CARTITUDE-1): a phase 1b/2 open-label study. *The Lancet* **398**, 314–324 (2021).

8. M. J. Buzon, H. Sun, C. Li, A. Shaw, K. Seiss, Z. Ouyang, E. Martin-Gayo, J. Leng, T. J. Henrich, J. Z. Li, F. Pereyra, R. Zurakowski, B. D. Walker, E. S. Rosenberg, X. G. Yu, M. Lichterfeld, HIV-1 persistence in CD4+ T cells with stem cell–like properties. *Nature Medicine* **20**, 139–142 (2014).
9. B. D. Preston, B. J. Poiesz, L. A. Loeb, Fidelity of HIV-1 reverse transcriptase. *Science* **242**, 1168–1171 (1988).
10. J. B. Dinoso, S. A. Rabi, J. N. Blankson, L. Gama, J. L. Mankowski, R. F. Siliciano, M. C. Zink, J. E. Clements, A Simian Immunodeficiency Virus-Infected Macaque Model To Study Viral Reservoirs That Persist during Highly Active Antiretroviral Therapy. *Journal of Virology* **83**, 9247–9257 (2009).
11. J. W. Rausch, S. F. J. Le Grice, Characterizing the Latent HIV-1 Reservoir in Patients with Viremia Suppressed on cART: Progress, Challenges, and Opportunities. *Curr HIV Res* **18**, 99–113 (2020).
12. A. Shen, M. C. Zink, J. L. Mankowski, K. Chadwick, J. B. Margolick, L. M. Carruth, M. Li, J. E. Clements, R. F. Siliciano, Resting CD4 ⁺ T Lymphocytes but Not Thymocytes Provide a Latent Viral Reservoir in a Simian Immunodeficiency Virus-Macaca nemestrina Model of Human Immunodeficiency Virus Type 1-Infected P. *Journal of Virology* **77**, 4938–4949 (2003).
13. R. T. Mitsuyasu, P. A. Anton, S. G. Deeks, D. T. Scadden, E. Connick, M. T. Downs, A. Bakker, M. R. Roberts, C. H. June, S. Jalali, A. A. Lin, R. Pennathur-Das, K. M. Hege, Prolonged survival and tissue trafficking following adoptive transfer of CD4ζ gene-modified autologous CD4+ and CD8+ T cells in human immunodeficiency virus–infected subjects. *Blood* **96**, 785–793 (2000).
14. S. G. Deeks, B. Wagner, P. A. Anton, R. T. Mitsuyasu, D. T. Scadden, C. Huang, C. Macken, D. D. Richman, C. Christopherson, C. H. June, R. Lazar, D. F. Broad, S. Jalali, K. M. Hege, A Phase II Randomized Study of HIV-Specific T-Cell Gene Therapy in Subjects with Undetectable Plasma Viremia on Combination Antiretroviral Therapy. *Molecular Therapy* **5**, 788–797 (2002).
15. L. Liu, B. Patel, M. H. Ghanem, V. Bundoc, Z. Zheng, R. A. Morgan, S. A. Rosenberg, B. Dey, E. A. Berger, Novel CD4-Based Bispecific Chimeric Antigen Receptor Designed for Enhanced Anti-HIV Potency and Absence of HIV Entry Receptor Activity. *Journal of Virology* **89**, 6685–6694 (2015).
16. K. Anthony-Gonda, A. Bardhi, A. Ray, N. Flerin, M. Li, W. Chen, C. Ochsenbauer, J. C. Kappes, W. Krueger, A. Worden, D. Schneider, Z. Zhu, R. Orentas, D. S. Dimitrov, H. Goldstein, B. Dropulić, Multispecific anti-HIV duoCAR-T cells display broad in vitro antiviral activity and potent in vivo elimination of HIV-infected cells in a humanized mouse model. *Science Translational Medicine* **11**, eaav5685 (2019).
17. K. Anthony-Gonda, A. Ray, H. Su, Y. Wang, Y. Xiong, D. Lee, A. Block, V. Chilunda, J. Weiselberg, L. Zemelko, Y. Y. Wang, S. Kleinsorge-Block, J. S. Reese, M. De Lima, C. Ochsenbauer, J. C. Kappes, D. S. Dimitrov, R. Orentas, S. G. Deeks, R. L. Rutishauser, J. W. Berman, H. Goldstein, B. Dropulić, In vivo killing of primary HIV-infected cells by peripheral-injected early memory–enriched anti-HIV duoCAR T cells. *JCI Insight* **7**, (2022).
18. M. C. Choudhary, J. C. Cyktor, S. A. Riddler, Advances in HIV-1-specific chimeric antigen receptor cells to target the HIV-1 reservoir. *Journal of Virus Eradication* **8**, 100073 (2022).

19. Y. Mao, Q. Liao, Y. Zhu, M. Bi, J. Zou, N. Zheng, L. Zhu, C. Zhao, Q. Liu, L. Liu, J. Chen, L. Gu, Z. Liu, X. Pan, Y. Xue, M. Feng, T. Ying, P. Zhou, Z. Wu, J. Xiao, R. Zhang, J. Leng, Y. Sun, X. Zhang, J. Xu, Efficacy and safety of novel multifunctional M10 CAR-T cells in HIV-1-infected patients: a phase I, multicenter, single-arm, open-label study. *Cell Discovery* **10**, 49 (2024).
20. R. E. Walker, C. M. Bechtel, V. Natarajan, M. Baseler, K. M. Hege, J. A. Metcalf, R. Stevens, A. Hazen, R. M. Blaese, C. C. Chen, S. F. Leitman, J. Palensky, J. Wittes, R. T. Davey, J. Falloon, M. A. Polis, J. A. Kovacs, D. F. Broad, B. L. Levine, M. R. Roberts, H. Masur, H. C. Lane, Long-term in vivo survival of receptor-modified syngeneic T cells in patients with human immunodeficiency virus infection. *Blood* **96**, 467–474 (2000).
21. S.-Y. Wang, G. M. Scurti, A. V. Dalheim, S. Quinn, P. J. Stiff, M. I. Nishimura, Nonactivated and IL-7 cultured CD19-specific CAR T cells are enriched in stem cell phenotypes and functionally superior. *Blood Advances* **8**, 324–335 (2024).
22. D. M. Barrett, N. Singh, X. Liu, S. Jiang, C. H. June, S. A. Grupp, Y. Zhao, Relation of clinical culture method to T-cell memory status and efficacy in xenograft models of adoptive immunotherapy. *Cytotherapy* **16**, 619–630 (2014).
23. Y. Kagoya, M. Nakatsugawa, T. Ochi, Y. Cen, T. Guo, M. Anczurowski, K. Saso, M. O. Butler, N. Hirano, Transient stimulation expands superior antitumor T cells for adoptive therapy. *JCI Insight* **2**, (2017).
24. J. A. Fraietta, S. F. Lacey, E. J. Orlando, I. Pruteanu-Malinici, M. Gohil, S. Lundh, A. C. Boesteanu, Y. Wang, R. S. O'Connor, W.-T. Hwang, E. Pequignot, D. E. Ambrose, C. Zhang, N. Wilcox, F. Bedoya, C. Dorfmeier, F. Chen, L. Tian, H. Parakandi, M. Gupta, R. M. Young, F. B. Johnson, I. Kulikovskaya, L. Liu, J. Xu, S. H. Kassim, M. M. Davis, B. L. Levine, N. V. Frey, D. L. Siegel, A. C. Huang, E. J. Wherry, H. Bitter, J. L. Brogdon, D. L. Porter, C. H. June, J. J. Melenhorst, Determinants of response and resistance to CD19 chimeric antigen receptor (CAR) T cell therapy of chronic lymphocytic leukemia. *Nature Medicine* **24**, 563–571 (2018).
25. L. Gattinoni, E. Lugli, Y. Ji, Z. Pos, C. M. Paulos, M. F. Quigley, J. R. Almeida, E. Gostick, Z. Yu, C. Carpenito, E. Wang, D. C. Douek, D. A. Price, C. H. June, F. M. Marincola, M. Roederer, N. P. Restifo, A human memory T cell subset with stem cell–like properties. *Nature Medicine* **17**, 1290–1297 (2011).
26. G. Oliveira, E. Ruggiero, M. T. L. Stanghellini, N. Cieri, M. D'Agostino, R. Fronza, C. Lulay, F. Dionisio, S. Mastaglio, R. Greco, J. Peccatori, A. Aiuti, A. Ambrosi, L. Biasco, A. Bondanza, A. Lambiase, C. Traversari, L. Vago, C. von Kalle, M. Schmidt, C. Bordignon, F. Ciceri, C. Bonini, Tracking genetically engineered lymphocytes long-term reveals the dynamics of T cell immunological memory. *Science Translational Medicine* **7**, 317ra198–317ra198 (2015).
27. S. Arcangeli, C. Bove, C. Mezzanotte, B. Camisa, L. Falcone, F. Manfredi, E. Bezzecchi, R. El Khoury, R. Norata, F. Sanvito, M. Ponzoni, B. Greco, M. A. Moresco, M. G. Carrabba, F. Ciceri, C. Bonini, A. Bondanza, M. Casucci, CAR T cell manufacturing from naive/stem memory T lymphocytes enhances antitumor responses while curtailing cytokine release syndrome. *Journal of Clinical Investigation* **132**, (2022).
28. E. Kranz, C. J. Kuhlmann, J. Chan, P. Y. Kim, I. S. Y. Chen, M. Kamata, Efficient derivation of chimeric-antigen receptor-modified T(SCM) cells. *Front Immunol* **13**, 877682 (2022).

29. L. Garcia-Garcia, G. S. E, M. Ivanova, K. Pastora, C. Alcantara-Sanchez, J. Garcia-Martinez, B. Martin-Antonio, M. Ramirez, A. Gonzalez-Murillo, Choosing T-cell sources determines CAR-T cell activity in neuroblastoma. *Front Immunol* **15**, 1375833 (2024).
30. L. Gattinoni, X. S. Zhong, D. C. Palmer, Y. Ji, C. S. Hinrichs, Z. Yu, C. Wrzesinski, A. Boni, L. Cassard, L. M. Garvin, C. M. Paulos, P. Muranski, N. P. Restifo, Wnt signaling arrests effector T cell differentiation and generates CD8+ memory stem cells. *Nat Med* **15**, 808–813 (2009).
31. Y. Zhao, J. Chen, M. Andreatta, B. Feng, Y.-Q. Xie, M. Wenes, Y. Wang, M. Gao, X. Hu, P. Romero, S. Carmona, J. Sun, Y. Guo, L. Tang, IL-10-expressing CAR T cells resist dysfunction and mediate durable clearance of solid tumors and metastases. *Nature Biotechnology*, (2024).
32. N. Shrestha, M. J. Dee, P. Chaturvedi, G. M. Leclerc, M. Mathyer, C. Dufour, L. Arthur, M. Becker-Hapak, M. Foster, E. McClain, N. V. Pena, K. Kage, X. Zhu, V. George, B. Liu, J. Egan, C. Echeverri, M. Wang, L. You, L. Kong, L. Li, M. M. Berrien-Elliott, M. L. Cooper, T. A. Fehniger, P. R. Rhode, H. C. Wong, A "Prime and Expand" strategy using the multifunctional fusion proteins to generate memory-like NK cells for cell therapy. *Cancer Immunology, Immunotherapy* **73**, (2024).
33. K. Seay, C. Church, J. H. Zheng, K. Deneroff, C. Ochsenbauer, J. C. Kappes, B. Liu, E. K. Jeng, H. C. Wong, H. Goldstein, In Vivo Activation of Human NK Cells by Treatment with an Interleukin-15 Superagonist Potently Inhibits Acute In Vivo HIV-1 Infection in Humanized Mice. *J Virol* **89**, 6264–6274 (2015).
34. W. J. Leonard, R. Spolski, Interleukin-21: a modulator of lymphoid proliferation, apoptosis and differentiation. *Nature Reviews Immunology* **5**, 688–698 (2005).
35. S. Cavalieri, S. Cazzaniga, M. Geuna, Z. Magnani, C. Bordignon, L. Naldini, C. Bonini, Human T lymphocytes transduced by lentiviral vectors in the absence of TCR activation maintain an intact immune competence. *Blood* **102**, 497–505 (2003).
36. S.-Y. Wang, T. V. Moore, A. V. Dalheim, G. M. Scurti, M. I. Nishimura, Melanoma reactive TCR-modified T cells generated without activation retain a less differentiated phenotype and mediate a superior in vivo response. *Scientific Reports* **11**, (2021).
37. H. Lee, S. Y. Kim, S. H. Kim, S. Jeong, K. H. Kim, C. G. Kim, J. Y. Koh, H. D. Kim, J. W. Han, H. Yu, W. Lee, S. Min, S. H. Park, H. S. Eun, E. C. Shin, TCR signaling via NFATc1 constrains IL-15-induced bystander activation of human memory CD8(+) T cells. *Immunity* **58**, 2957–2971 e2958 (2025).
38. N. Cieri, B. Camisa, F. Cocchiarella, M. Forcato, G. Oliveira, E. Provasi, A. Bondanza, C. Bordignon, J. Peccatori, F. Ciceri, M. T. Lupo-Stanghellini, F. Mavilio, A. Mondino, S. Bicciato, A. Recchia, C. Bonini, IL-7 and IL-15 instruct the generation of human memory stem T cells from naive precursors. *Blood* **121**, 573–584 (2013).
39. C. M. Carlson, B. T. Endrizzi, J. Wu, X. Ding, M. A. Weinreich, E. R. Walsh, M. A. Wani, J. B. Lingrel, K. A. Hogquist, S. C. Jameson, Kruppel-like factor 2 regulates thymocyte and T-cell migration. *Nature* **442**, 299–302 (2006).
40. C. T. Kuo, M. L. Veselits, J. M. Leiden, LKLF: A Transcriptional Regulator of Single-Positive T Cell Quiescence and Survival. *Science* **277**, 1986–1990 (1997).
41. S. Liang, R. Zheng, B. Zuo, J. Li, Y. Wang, Y. Han, H. Dong, X. Zhao, Y. Zhang, P. Wang, R. Meng, L. Jia, A. Yang, B. Yan, SMAD7 expression in CAR-T cells improves persistence and safety for solid tumors. *Cell Mol Immunol* **21**, 213–226 (2024).

42. F. B. Aiello, L. Graciotti, A. D. Procopio, J. R. Keller, S. K. Durum, Stemness of T cells and the hematopoietic stem cells: fate, memory, niche, cytokines. *Cytokine Growth Factor Rev* **24**, 485–501 (2013).
43. A. Drake, M. Kaur, B. P. Iliopoulou, R. Phennicie, A. Hanson, J. Chen, Interleukins 7 and 15 Maintain Human T Cell Proliferative Capacity through STAT5 Signaling. *PLOS ONE* **11**, e0166280 (2016).
44. L. D. Shultz, B. L. Lyons, L. M. Burzenski, B. Gott, X. Chen, S. Chaleff, M. Kotb, S. D. Gillies, M. King, J. Mangada, D. L. Greiner, R. Handgretinger, Human Lymphoid and Myeloid Cell Development in NOD/LtSz-scid IL2Rγnull Mice Engrafted with Mobilized Human Hemopoietic Stem Cells. *The Journal of Immunology* **174**, 6477–6489 (2005).
45. J. K. Flynn, P. R. Gorry, Stem memory T cells (TSCM)—their role in cancer and HIV immunotherapies. *Clinical & Translational Immunology* **3**, e20 (2014).
46. C. S. Hinrichs, Z. A. Borman, L. Cassard, L. Gattinoni, R. Spolski, Z. Yu, L. Sanchez-Perez, P. Muranski, S. J. Kern, C. Logun, D. C. Palmer, Y. Ji, R. N. Reger, W. J. Leonard, R. L. Danner, S. A. Rosenberg, N. P. Restifo, Adoptively transferred effector cells derived from naïve rather than central memory CD8 ⁺ T cells mediate superior antitumor immunity. *Proceedings of the National Academy of Sciences* **106**, 17469–17474 (2009).
47. R. J. Hodes, K. S. Hathcock, N.-P. Weng, Telomeres in T and B cells. *Nature Reviews Immunology* **2**, 699–706 (2002).
48. S. Liu, G. Lizée, Y. Lou, C. Liu, W. W. Overwijk, G. Wang, P. Hwu, IL-21 synergizes with IL-7 to augment expansion and anti-tumor function of cytotoxic T cells. *Int Immunol* **19**, 1213–1221 (2007).
49. Y. Shi, W. Wu, T. Wan, Y. Liu, G. Peng, Z. Chen, H. Zhu, Impact of polyclonal anti-CD3/CD28-coated magnetic bead expansion methods on T cell proliferation, differentiation and function. *Int Immunopharmacol* **15**, 129–137 (2013).
50. N. Watanabe, F. Mo, M. K. McKenna, Impact of Manufacturing Procedures on CAR T Cell Functionality. *Frontiers in Immunology* **13**, (2022).
51. Y. Xu, M. Zhang, C. A. Ramos, A. Durett, E. Liu, O. Dakhova, H. Liu, C. J. Creighton, A. P. Gee, H. E. Heslop, C. M. Rooney, B. Savoldo, G. Dotti, Closely related T-memory stem cells correlate with in vivo expansion of CAR.CD19-T cells and are preserved by IL-7 and IL-15. *Blood* **123**, 3750–3759 (2014).
52. S. Ghassemi, J. S. Durgin, S. Nunez-Cruz, J. Patel, J. Leferovich, M. Pinzone, F. Shen, K. D. Cummins, G. Plesa, V. A. Cantu, S. Reddy, F. D. Bushman, S. I. Gill, U. O'Doherty, R. S. O'Connor, M. C. Milone, Rapid manufacturing of non-activated potent CAR T cells. *Nature Biomedical Engineering* **6**, 118–128 (2022).
53. Y. Li, Y. Cong, M. Jia, Q. He, H. Zhong, Y. Zhao, H. Li, M. Yan, J. You, J. Liu, L. Chen, H. Hang, S. Wang, Targeting IL-21 to tumor-reactive T cells enhances memory T cell responses and anti-PD-1 antibody therapy. *Nature Communications* **12**, 951 (2021).
54. C. Alvarez-Fernández, L. Escribà-Garcia, S. Vidal, J. Sierra, J. Briones, A short CD3/CD28 costimulation combined with IL-21 enhance the generation of human memory stem T cells for adoptive immunotherapy. *Journal of Translational Medicine* **14**, (2016).
55. C. S. Hinrichs, R. Spolski, C. M. Paulos, L. Gattinoni, K. W. Kerstann, D. C. Palmer, C. A. Klebanoff, S. A. Rosenberg, W. J. Leonard, N. P. Restifo, IL-2 and IL-21 confer

opposing differentiation programs to CD8+ T cells for adoptive immunotherapy. *Blood* **111**, 5326–5333 (2008).
56. L. Du, Y. Nai, M. Shen, T. Li, J. Huang, X. Han, W. Wang, D. Pang, A. Jin, IL-21 Optimizes the CAR-T Cell Preparation Through Improving Lentivirus Mediated Transfection Efficiency of T Cells and Enhancing CAR-T Cell Cytotoxic Activities. *Frontiers in Molecular Biosciences* **8**, (2021).
57. W. Xu, M. Jones, B. Liu, X. Zhu, C. B. Johnson, A. C. Edwards, L. Kong, E. K. Jeng, K. Han, W. D. Marcus, M. P. Rubinstein, P. R. Rhode, H. C. Wong, Efficacy and mechanism-of-action of a novel superagonist interleukin-15: interleukin-15 receptor αSu/Fc fusion complex in syngeneic murine models of multiple myeloma. *Cancer Res* **73**, 3075–3086 (2013).
58. Y. Cihui, C. Jingjing, S. Xinmiao, Y. Fan, Y. Wenwen, A. Yang, W. Feng, Y. Lili, R. Xiubao, Memory stem T cells generated by Wnt signaling from blood of human renal clear cell carcinoma patients. *Cancer Biology & Medicine* **16**, 109 (2019).
59. S. Nüssing, L. A. Miosge, K. Lee, M. Olshansky, A. Barugahare, C. M. Roots, Y. Sontani, E. B. Day, M. Koutsakos, K. Kedzierska, C. C. Goodnow, B. E. Russ, S. R. Daley, S. J. Turner, SATB1 ensures appropriate transcriptional programs within naïve CD8⁺ T cells. *Immunology & Cell Biology* **100**, 636–652 (2022).
60. B. E. Russ, A. Barugahare, P. Dakle, K. Tsyganov, S. Quon, B. Yu, J. Li, J. K. C. Lee, M. Olshansky, Z. He, P. F. Harrison, M. See, S. Nussing, A. E. Morey, V. A. Udupa, T. J. Bennett, A. Kallies, C. Murre, P. Collas, D. Powell, A. W. Goldrath, S. J. Turner, Active maintenance of CD8+ T cell naivety through regulation of global genome architecture. *Cell Reports* **42**, 113301 (2023).
61. S. Lin, H. Niu, Y. Zhang, K. Gai, R. Brown, A. Brown, J. Shen, Z. Xu, R. K. Shah, J. L. Schmeling, M. Vargas-Cortes, A. E. Zamora, T. Kohwi-Shigematsu, J. Fan, B. Zhang, W. Cui, SATB1 is a key regulator of quiescence in stem-like CD8+ T cells. *Nature Immunology*, (2025).
62. D. D. Scripture-Adams, D. G. Brooks, Y. D. Korin, J. A. Zack, Interleukin-7 induces expression of latent human immunodeficiency virus type 1 with minimal effects on T-cell phenotype. *J Virol* **76**, 13077–13082 (2002).
63. C. Vandergeeten, R. Fromentin, S. DaFonseca, M. B. Lawani, I. Sereti, M. M. Lederman, M. Ramgopal, J. P. Routy, R. P. Sékaly, N. Chomont, Interleukin-7 promotes HIV persistence during antiretroviral therapy. *Blood* **121**, 4321–4329 (2013).
64. A. Bosque, M. Famiglietti, A. S. Weyrich, C. Goulston, V. Planelles, Homeostatic proliferation fails to efficiently reactivate HIV-1 latently infected central memory CD4+ T cells. *PLoS Pathog* **7**, e1002288 (2011).
65. R. B. Jones, S. Mueller, R. O'Connor, K. Rimpel, D. D. Sloan, D. Karel, H. C. Wong, E. K. Jeng, A. S. Thomas, J. B. Whitney, S.-Y. Lim, C. Kovacs, E. Benko, S. Karandish, S.-H. Huang, M. J. Buzon, M. Lichterfeld, A. Irrinki, J. P. Murry, A. Tsai, H. Yu, R. Geleziunas, A. Trocha, M. A. Ostrowski, D. J. Irvine, B. D. Walker, A Subset of Latency-Reversing Agents Expose HIV-Infected Resting CD4+ T-Cells to Recognition by Cytotoxic T-Lymphocytes. *PLOS Pathogens* **12**, e1005545 (2016).
66. J. S. Miller, Z. B. Davis, E. Helgeson, C. Reilly, A. Thorkelson, J. Anderson, N. S. Lima, S. Jorstad, G. T. Hart, J. H. Lee, J. T. Safrit, H. Wong, S. Cooley, L. Gharu, H. Chung, P. Soon-Shiong, C. Dobrowolski, C. V. Fletcher, J. Karn, D. C. Douek, T. W. Schacker,

Safety and virologic impact of the IL-15 superagonist N-803 in people living with HIV: a phase 1 trial. *Nat Med* **28**, 392–400 (2022).

67. M. Li, S. J. Garforth, K. E. O'Connor, H. Su, D. M. Lee, A. Celikgil, R. J. Chaparro, R. D. Seidel, R. B. Jones, R. Arav-Boger, S. C. Almo, H. Goldstein, T cell receptor–targeted immunotherapeutics drive selective in vivo HIV- and CMV-specific T cell expansion in humanized mice. *Journal of Clinical Investigation* **131**, (2021).

68. A. Joseph, J. H. Zheng, A. Follenzi, T. DiLorenzo, K. Sango, J. Hyman, K. Chen, A. Piechocka-Trocha, C. Brander, E. Hooijberg, D. A. Vignali, B. D. Walker, H. Goldstein, Lentiviral Vectors Encoding Human Immunodeficiency Virus Type 1 (HIV-1)-Specific T-Cell Receptor Genes Efficiently Convert Peripheral Blood CD8 T Lymphocytes into Cytotoxic T Lymphocytes with Potent In Vitro and In Vivo HIV-1-Specific Inhibitory Activity. *Journal of Virology* **82**, 3078–3089 (2008).

69. A. Bardhi, Y. Wu, W. Chen, W. Li, Z. Zhu, J. H. Zheng, H. Wong, E. Jeng, J. Jones, C. Ochsenbauer, J. C. Kappes, D. S. Dimitrov, T. Ying, H. Goldstein, Potent In Vivo NK Cell-Mediated Elimination of HIV-1-Infected Cells Mobilized by a gp120-Bispecific and Hexavalent Broadly Neutralizing Fusion Protein. *Journal of Virology* **91**, 10.1128/jvi.00937–00917 (2017).

70. T. G. Edmonds, H. Ding, X. Yuan, Q. Wei, K. S. Smith, J. A. Conway, L. Wieczorek, B. Brown, V. Polonis, J. T. West, D. C. Montefiori, J. C. Kappes, C. Ochsenbauer, Replication competent molecular clones of HIV-1 expressing Renilla luciferase facilitate the analysis of antibody inhibition in PBMC. *Virology* **408**, 1–13 (2010).

Acknowledgements:

We thank Drs. John Kappes and Christina Ochsenbauer for the development and sharing of the Env-IMC-LucR HIV-1 virus system. HIV-1 JR-CSF was obtained through the NIH HIV Reagent Program, Division of AIDS, National Institute of Allergy and Infectious Diseases (NIAID), National Institutes of Health (NIH). We acknowledge the support of the Albert Einstein College of Medicine Macromolecular Therapeutics Development Facility and Flow Cytometry Core, both supported by the Einstein National Cancer Institute Cancer Center Support Grant P30CA013330. We thank the BRB Preclinical Repository (Developmental Therapeutics Program, National Cancer Institute) for providing IL-2, Dr. Melissa Fazzari for statistical support, and Cecilia Knowles for assistance with CD19 CAR intracellular cytokine staining experiments. We also thank members of the laboratory for their support and expertise. H.G. acknowledges support from the Charles Michael Chair in Autoimmune Diseases. This work was supported by the National Institutes of Health through grants R01AI172607 and R01AI174275 (H.G.); the Einstein–Rockefeller–CUNY Center for AIDS Research grant P30AI124414 (H.G.), supported by the NIH co-funding and participating Institutes and Centers including the National Institute of Allergy and Infectious Diseases, National Cancer Institute, Eunice Kennedy Shriver National Institute of Child Health and Human Development, National Heart, Lung, and Blood Institute, National Institute on Drug Abuse, National Institute of Mental Health, National Institute on Aging, Fogarty International Center, and the Office of AIDS Research; T32AI007501 (E.B.C., C.R.H.); R01CA263079 (C.C.Z.); and the National Center for Advancing Translational Sciences grant UL1TR001866 (H.B.H., M.K.). The HCW9206 cytokine scaffold can be provided by HCW Biologics pending scientific review and a completed material transfer agreement.

Requests for the HCW9206 should be submitted to: Dr. Niraj Shrestha (NirajShrestha@hcwbiologics.com).

Funding:

National Institutes of Health grant R01AI172607 (H.G.)

National Institutes of Health grant R01AI174275 (H.G.)

Einstein-Rockefeller-CUNY Center for AIDS Research grant P30 AI124414, supported by the NIH Co-Funding and Participating Institutes and Centers: NIAID, NCI, NICHD, NHLBI, NIDA, NIMH, NIA, FIC, and OAR. (H.G.)

National Institutes of Health grant T32AI007501 (E.B.C., C.R.H.)

National Institutes of Health grant R01CA263079 (C.C.Z.)

National Center for Advancing Translational Sciences (NCATS) grant UL1TR001866 (H.B.H. and M.K.)

Author Contributions:

Conceptualization: E.B.C., H.G., N.S., H.C.W., B.D., A.V.S., C.R.H.

Methodology: E.B.C., H.G., H.C.W., N.S., M.K., N.V.P., A.V.S., C.R.H., Y.X., Z.Z.

Investigation: E.B.C., S.L., A.V.S., A.G.V., C.R.H., J.Z., Y.X., H.C.W.

Resources: H.G., B.D., N.S., H.C.W., A.V.S., Y.X., M.K., C.C.Z., N.V.P., Z.Z.

Data curation: E.B.C., M.K., A.V.S.

Validation: E.B.C., S.L., A.V.S., Y.X., M.K., C.R.H., H.C.W., J.Z.

Formal analysis: E.B.C., M.K., H.C.W., A.G.V., H.B.H., J.Z.

Software: M.K., H.B.H.

Visualization: E.B.C., M.K., H.B.H.

Writing – original draft: E.B.C., H.G.

Writing – review & editing: E.B.C., H.G., S.L., N.S., A.V.S., A.G.V., C.R.H., Y.X., Z.Z., M.K., H.B.H., C.C.Z., H.C.W.

Supervision: N.S., M.K., C.C.Z., H.G., H.C.W.

Funding acquisition: H.G., H.C.W., C.C.Z.

Project administration: H.G., E.B.C., H.C.W., C.C.Z.

Competing interests:

H.C.W., N.S., and N.V.P. are inventors on a patent related to this work filed by HCW Biologics Inc. (No. 11,884,712, Filed 30 June 2023, Published 14 December 2023). E.B.C., H.G., H.C.W., and N.S. are inventors on a patent application related to this work filed by HCW Biologics Inc. (No. 63/798,533, Filed 5 January 2025). B.D. is an inventor on a patent related to this work filed by Lentigen Technology Inc. (No. 10,894,819 B2, Filed 20 December 2018, Published 19 January 2021). The authors declare no other competing interests.

Data and materials availability:

The HCW9206 scaffold can be provided by HCW Biologics, Inc., pending scientific review and a completed material transfer agreement. Requests for the HCW9206 should be submitted to: Dr. Niraj Shrestha (NirajShrestha@hcwbiologics.com). All data needed to evaluate and reproduce the results in the paper are present in the paper and/or the Supplementary Materials. Sequencing data have been deposited in the NCBI Gene Expression Omnibus (GEO) under accession number GSE314278.

Figure Legends

Figure 1: HCW9206 cytokine scaffold stimulates human T-cells in vitro. (**A**) Schematic of HCW9206. (**B**) Representative histogram plot depicting phospho-STAT5 or phospho-STAT3 expression in $CD8^+$ T-cells following HCW9206 (100nM) stimulation. (**C**) phospho-STAT5 expression represented by MFI (N = 3) following stimulation with HCW9206 (100nM), IL-15, IL-7, IL-21 (1nM) or no stimulation. (**D**) phospho-STAT3 expression represented by MFI (N = 3). (**E**) Representative histogram plots from one donor (HGLK00122) showing proliferation of human $CD8^+$ T-cells and $T_{N/SCM}$ memory populations after Cell Trace Violet (CTV) staining following αCD3/C28 activation or HCW9206 (100nM) treatment ($T_{N/SCM}$: $CD45RO^-CCR7^+$). (**F**) % proliferating $CD8^+$ T-cells following 7-day αCD3/28 stimulation or HCW9206 treatment. Gated on Lymphocytes, Single Cells, $CD8^+$, CTV^- (N = 4). (**G**) % proliferating $CD8^+$ T_{SCM} cells following αCD3/28 stimulation or HCW9206 treatment. Gated on Lymphocytes, Single Cells, $CD8^+$, $CD45RO^-$, $CCR7^+$, CTV^- (N = 4). Data are represented as mean ± SEM. Statistical analysis performed by one-way ANOVA (**C-D**) or unpaired t-test (**F-G**). Created in BioRender. Cole, E. (2026). https://BioRender.com/pqy742r

<u>Figure 2:</u> HCW9206 treatment enables T-cell lentiviral transduction to generate HIV-specific duoCAR-T cells. (**A**) Representation of anti-HIV duoCAR and packaging plasmid maps. (**B**) Protocol for HCW9206-generated anti-HIV duoCAR-T cell product. Briefly, T-cells were treated with HCW9206 for 7-days or activated with αCD3/28 for 3-days prior to transduction with CAR-LV. (**C**) Representative FACS dot and histogram plots showing $CD8^+$ T-cell-expression of m36.4 and mD1.22 duoCAR following treatment with HCW9206 (100nM) or αCD3/28+IL-2 (100U/mL). (**D**) duoCAR expression in age-matched donor $CD8^+$ T-cells after αCD3/28-activation or HCW9206- or soluble cytokine-treatment (N = 3). Gated on Lymphocytes, Single Cells, $CD8^+$, $m36.4^+$ (N = 3). (**E**) Frequency of $CD8^+$ duoCAR-T_{SCM} cells following αCD3/28-activation or cytokine-treatment. Gated on Lymphocytes, Single Cells, $CD8^+$, $m36.4^+$, $CD45RO^–$, $CCR7^+$, $CD95^+$ (N = 3). Statistical analysis compared to HCW9206. (**F**) Progeny assay depicting frequency changes in duoCAR-T cell memory populations of αCD3/28-activated or HCW9206-treated duoCAR-T cells before and after 4-day-stimulation with 293T-gp120 cells (E:T - 2:1) (N = 3). Data is shown as mean ± SEM of triplicates and statistical analysis was performed by one-way (**D-E**) or two-way ANOVA (**F**). Created in BioRender. Cole, E. (2026). https://BioRender.com/pqy742r

<u>Figure 3:</u> HCW9206 treatment of T-cells to generate T_{SCM}-enriched CD19-specific CAR-T cells. (**A**) Representation of the CD19-CAR and packaging plasmid maps. (**B**) % CAR expression in age-matched donor $CD8^+$ T-cells after αCD3/28-activation or HCW9206 (100nM)-, IL-15- or IL-2 (1nM)-treatment (N = 3). (**C**) Representative FACS contour plot of the T-cell memory phenotype of $CD8^+$ CD19-CAR-T cells generated from either αCD3/28-activation or HCW9206-stimulation (left panel). Histogram plots depicting upregulation of T_{SCM} markers (CD95 and CD45RA) within the HCW9206 CD19-CAR-$T_{N/SCM}$ population ($T_{N/SCM}$: $CD45RO^-$ $CCR7^+$) (right panel) (**D**) $CD8^+$ CD19-CAR-T_{SCM} cell frequency in age-matched donors. Gated on Lymphocytes, Single Cells, $CD8^+$, GFP^+, $CD45RO^-$, $CCR7^+$, $CD95^+$ (N = 3). Statistical analysis compared to HCW9206-treatment. (**E**) $CD8^+$ CD19-CAR-T_{SCM} cells frequency comparing IL-7-stimulation (1nM) to HCW9206-treatment (1nM , 100nM) (N = 3). (**F**) Progeny analysis depicting frequency changes in CD19-CAR-T cell memory populations before and after NALM-6 cell-stimulation (N = 3). Data are shown as the mean ± SEM of triplicates, and statistical analysis was performed using one-way ANOVA (B, D), one-way repeated measures ANOVA (E), or two-way ANOVA (**F**). Created in BioRender. Cole, E. (2026). https://BioRender.com/pqy742r

Figure 4: HCW9206 stimulation generates cytotoxic and polyfunctional HIV- and CD19-specific CAR-T cells. (**A-B**) In vitro killing efficacy by duoCAR-$T_{\alpha CD3/28}$ and duoCAR-$T_{HCW9206}$ cells against autologous HIV-1-infected $CD4^+$ T-cells with HIV-LucR IMC expressing (**A**) JRCSF or (**B**) BaL envelope. Anti-HIV activity is measured as % HIV-1 suppression compared to untreated HIV-1-infected T-cells. HIV-infection post co-culture with duoCAR-T cells or UTD T-cells (E:T - 1:10, 1:20, 1:40) was quantified via *Renilla* luciferase activity (*y* axis; relative light units, RLU) (N = 3). (**C-D**) In vitro short-term EuTDA cytotoxicity assay comparing CD19-CAR-$T_{\alpha CD3/28}$ and CD19-CAR-$T_{HCW9206}$ cells. % specific lysis is measured after 3-hour co-culture of CD19-CAR-T cells with (**C**) $CD19^+$ Raji or (**D**) NALM-6 cells at different E:T ratios (N = 5). (**E**) Flow cytometric quantification of duoCAR-$T_{\alpha CD3/28}$ or duoCAR-$T_{HCW9206}$ cell-production of indicated cytokines or (**F**) production of IFNγ or (**G**) TNFα by $CD8^+$ T_{EM} or T_{SCM} populations after 16-hour co-culture with 293T-gp120 cells. (**H**) Flow cytometric quantification of CD19-CAR-$T_{\alpha CD3/28}$ or CD19-CAR-$T_{HCW9206}$ cell-production of indicated cytokines or (**I**) production of IFNγ or (**J**) TNFα by $CD8^+$ T_{EM} or T_{SCM} subpopulations after 16-hour co-culture with NALM-6 cells. Created in BioRender. Cole, E. (2026). https://BioRender.com/pqy742r

<u>Figure 5:</u> HCW9206-generated HIV-specific duoCAR-T cells display both T_{SCM}-like and effector-like transcriptional programming (**A**) Experimental protocol and timeline (days). (**B**) Venn diagram of DEGs identified for comparison of duoCAR-$T_{\alpha CD3/28}$ vs. duoCAR-$T_{HCW9206}$ cells in unstimulated (293T-incubated) and antigen-stimulated (293T-gp120-incubated) duoCAR-T cells. (**C-D**) Heatmap of T-cell activation- and development-associated DEGs in (**C**) duoCAR-$T_{HCW9206}$ cells+293T vs. duoCAR-$T_{\alpha CD3/28}$ cells+293T and (**D**) duoCAR-$T_{HCW9206}$ cells+293T-gp120 vs. duoCAR-$T_{\alpha CD3/28}$ cells+293T-gp120 comparisons. DEGs were identified through Ingenuity Pathway Analysis (IPA) (padj ≤ 0.05; $|\log2(FC)| \geq 1$; $|z\text{-score}| \geq 2$) (N = 2). (**E**) The top 35 IPA downstream functions predicted for the DEGs in duoCAR-$T_{HCW9206}$ vs. duoCAR-$T_{\alpha CD3/28}$ cells cultured with 293T. Predictions are ranked from the lowest z-score value to the highest z-score value, with z-score values identified using Fisher's exact test. Created in BioRender. Cole, E. (2026). https://BioRender.com/pqy742r

<u>Figure 6:</u> CD19-CAR-T$_{HCW9206}$ cells suppress NALM-6 cell expansion longer than CD19-CAR-T$_{\alpha CD3/28}$ cells and display increased functional persistence in NSG mice. (**A**) Experimental protocol. NSG mice injected with Firefly Luciferase^{+} NALM-6 leukemia cells were treated with CD19-CAR-T$_{HCW9206}$ cells (n = 5), CD19-CAR-T$_{\alpha CD3/28}$ cells (n = 6), or UTD control T-cells (n = 10). (**B**) Representative bioluminescent scans of mice taken at indicated times. (**C**) Quantification of tumor burden by NALM-6 *Firefly* luciferase signal comparing CD19-CAR-T$_{HCW9206}$ cell-treated to CD19-CAR-T$_{\alpha CD3/28}$ cell-treated mice. Firefly luciferase activity or total photon flux is measured in relative light units (RLU). (**D**) CD8^{+}GFP^{+} CD19-CAR-T-cell expansion in the peripheral blood of tumor-bearing mice measured at indicated times after treatment. (**E-F**) T-cell memory phenotype of (**E**) CD19-CAR-T$_{HCW9206}$ or (**F**) CD19-CAR-T$_{\alpha CD3/28}$ cells in peripheral blood determined at the indicated times. (**G-H**) CD8^{+} CD19-CAR-T cell persistence in (**G**) spleen and (**H**) bone marrow of NALM-6 cell-injected mice measured on at 44-day endpoint. The ROUT method was used to identify and exclude outliers with a Q value of 1%. Data are represented as mean ± SEM. Statistical analysis performed by two-way ANOVA (**C-D**) or unpaired t-test (**G-H**). Created in BioRender. Cole, E. (2026). https://BioRender.com/pqy742r

<u>Figure 7:</u> HCW9206-generated anti-HIV duoCAR-Ts display more potent in vivo HIV-1 suppression compared to αCD3/28-generated duoCAR-Ts. (**A**) Experimental protocol using the hu-spl-PBMC-NSG-humanized mouse model of HIV-1 infection. NSG mice were injected with autologous HIV-1 JRCSF-infected PBMCs and treated with duoCAR-$T_{HCW9206}$ cells (n = 5), duoCAR-$T_{\alpha CD3/28}$ cells (n = 6), UTD control T-cells (n = 13), or untreated (HIV^+; n = 9) for 17-18 days. Mice injected with uninfected PBMCs served as a negative control (HIV^-; n = 5) (N = 2 donors). (**B**) Quantification of cell-associated total anti-HIV duoCAR DNA in the spleens of mice at endpoint expressed as duoCAR DNA copies per 1 million splenocytes. (**C**) Quantification of cell-associated total HIV-1 DNA in the spleens of mice at the study endpoint expressed as HIV-1 Gag DNA copies/10^6 splenocytes. (**D**) % human $CD4^+$ T cells detected at the endpoint by FACS analysis in the spleens of HIV-1-infected mice. Data is represented as mean ± SEM. Statistical analysis performed by parametric unpaired t-test (**B**) or by nonparametric (**C**) or parametric (**D**) one-way ANOVA compared to control (HIV^+). Created in BioRender. Cole, E. (2026). https://BioRender.com/pqy742r

<u>Figure 8:</u> Potent HCW9206-enriched duoCAR-T_{SCM}s can be generated from T-cells derived from PLWH. (**A**) Percent duoCAR expression in PLWH donor-derived $CD8^+$ T-cells. Gated on Lymphocytes, Single Cells, $CD3^+$, $CD8^+$, $m36.4^+$. (**B**) Representative contour plot of the T-cell memory phenotype of duoCAR-T cells generated by either αCD3/28 activation or HCW9206 stimulation (left panel). Right panel shows upregulation of two T_{SCM} markers (CD95 and CD27) within the HCW9206 duoCAR-$T_{N/SCM}$ population ($T_{N/SCM}$: $CD45RO^-CCR7^+$). (**C**) % duoCAR-T cells that are T_{SCM} cells. Gated on Lymphocytes, Single Cells, $CD3^+$, $CD8^+$, $m36.4^+$, $CD45RO^-$, $CCR7^+$, $CD95^+$ (N = 6). (**D**) Representative graph of PLWH donor (HGLK0072) showing HIV-1-LucR-BaL suppression at an E:T ratio of 1:1. The *y* axis displays the magnitude of HIV infection as a measure of *Renilla* luciferase (LucR) signal and is recorded as relative light units (RLU). PBMCs superinfected with HIV-1-LucR-BaL serve as a positive control (HIV^+), and uninfected PBMCs serve as a negative control (HIV^-). (**E**) % HIV-1-LucR-BaL suppression was calculated as compared to HIV^+ (N = 3). Data is shown as mean ± SEM. Statistical analysis performed by unpaired t test (**A, C, E**) or one-way ANOVA (**D**). Created in BioRender. Cole, E. (2026). https://BioRender.com/pqy742r

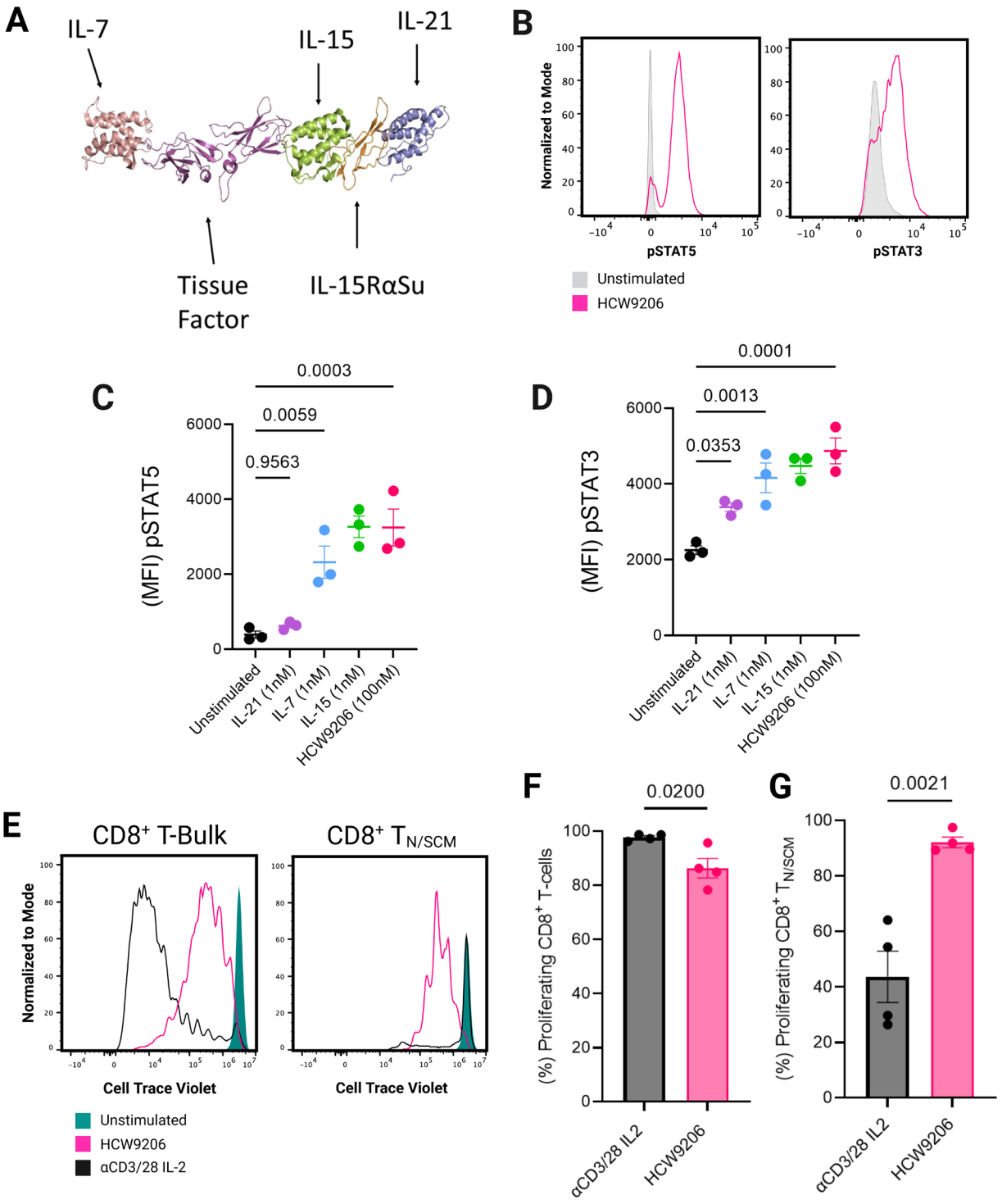
A
IL-7
IL-15
IL-21
Tissue Factor
IL-15RαSu
B
Normalized to Mode
pSTAT5
pSTAT3
Unstimulated
HCW9206
C
0.0003
0.0059
0.9563
(MFI) pSTAT5
Unstimulated
IL-21 (1nM)
IL-7 (1nM)
IL-15 (1nM)
HCW9206 (100nM)
D
0.0001
0.0013
0.0353
(MFI) pSTAT3
E
CD8⁺ T-Bulk
CD8⁺ T N/SCM
Cell Trace Violet
Unstimulated
HCW9206
αCD3/28 IL-2
F
0.0200
(%) Proliferating CD8⁺ T-cells
αCD3/28 IL2
HCW9206
G
0.0021
(%) Proliferating CD8⁺ T N/SCM

1401

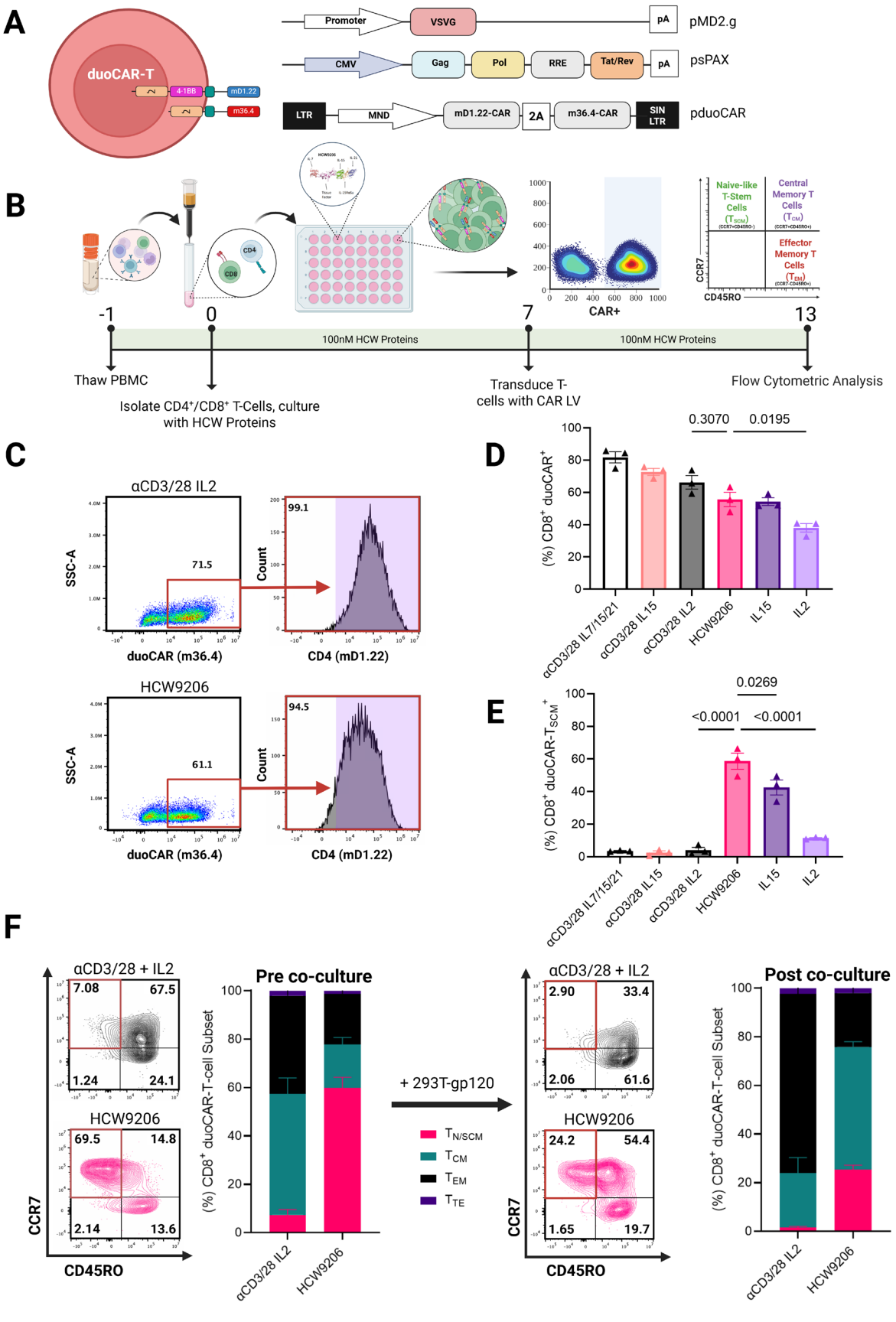
A
duoCAR-T
4-1BB
mD1.22
m36.4
Promoter
VSVG
pA
pMD2.g
CMV
Gag
Pol
RRE
Tat/Rev
pA
psPAX
LTR
MND
mD1.22-CAR
2A
m36.4-CAR
SIN LTR
pduoCAR
B
CD4
CD8
CAR+
Naive-like T-Stem Cells (TSCM)
Central Memory T Cells (TCM)
Effector Memory T Cells (TEM)
CCR7
CD45RO
-1
0
7
13
100nM HCW Proteins
100nM HCW Proteins
Thaw PBMC
Isolate CD4+/CD8+ T-Cells, culture with HCW Proteins
Transduce T-cells with CAR LV
Flow Cytometric Analysis
C
αCD3/28 IL2
SSC-A
71.5
duoCAR (m36.4)
Count
99.1
CD4 (mD1.22)
HCW9206
SSC-A
61.1
duoCAR (m36.4)
Count
94.5
CD4 (mD1.22)
D
0.3070
0.0195
(%) CD8+ duoCAR+
αCD3/28 IL7/15/21
αCD3/28 IL15
αCD3/28 IL2
HCW9206
IL15
IL2
E
0.0269
<0.0001
<0.0001
(%) CD8+ duoCAR-TSCM+
αCD3/28 IL7/15/21
αCD3/28 IL15
αCD3/28 IL2
HCW9206
IL15
IL2
F
αCD3/28 + IL2
7.08
67.5
1.24
24.1
HCW9206
69.5
14.8
2.14
13.6
CCR7
CD45RO
Pre co-culture
(%) CD8+ duoCAR-T-cell Subset
αCD3/28 IL2
HCW9206
+ 293T-gp120
TN/SCM
TCM
TEM
TTE
αCD3/28 + IL2
2.90
33.4
2.06
61.6
HCW9206
24.2
54.4
1.65
19.7
CCR7
CD45RO
Post co-culture
(%) CD8+ duoCAR-T-cell Subset
αCD3/28 IL2
HCW9206

1402

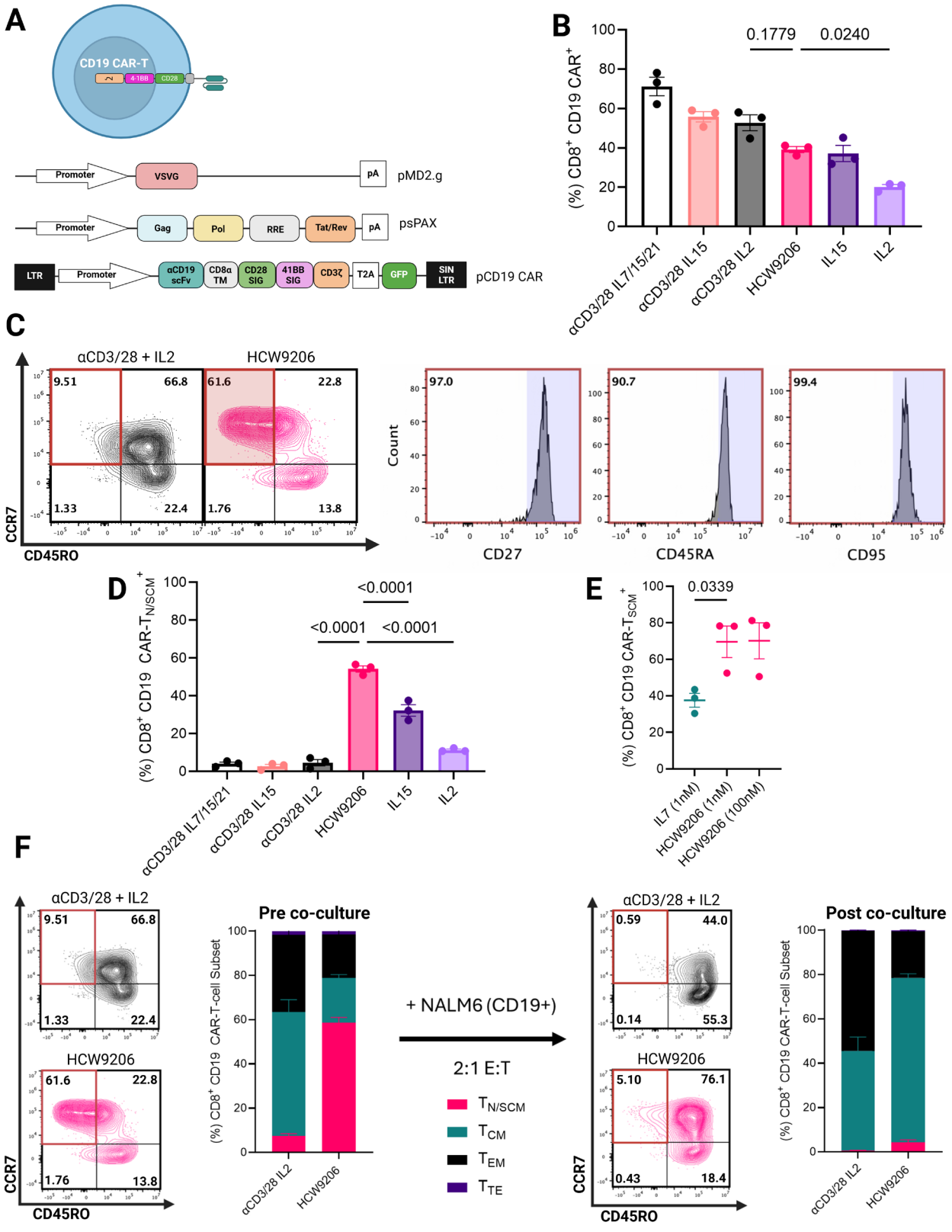
A
CD19 CAR-T
ζ
4-1BB
CD28
Promoter
VSVG
pA
pMD2.g
Promoter
Gag
Pol
RRE
Tat/Rev
pA
psPAX
LTR
Promoter
αCD19 scFv
CD8α TM
CD28 SIG
41BB SIG
CD3ζ
T2A
GFP
SIN LTR
pCD19 CAR
B
(%) CD8+ CD19 CAR+
0.1779
0.0240
αCD3/28 IL7/15/21
αCD3/28 IL15
αCD3/28 IL2
HCW9206
IL15
IL2
C
αCD3/28 + IL2
HCW9206
9.51
66.8
1.33
22.4
61.6
22.8
1.76
13.8
CCR7
CD45RO
97.0
90.7
99.4
Count
CD27
CD45RA
CD95
D
(%) CD8+ CD19 CAR-TN/SCM+
<0.0001
<0.0001
<0.0001
αCD3/28 IL7/15/21
αCD3/28 IL15
αCD3/28 IL2
HCW9206
IL15
IL2
E
(%) CD8+ CD19 CAR-TSCM+
0.0339
IL7 (1nM)
HCW9206 (1nM)
HCW9206 (100nM)
F
αCD3/28 + IL2
9.51
66.8
1.33
22.4
HCW9206
61.6
22.8
1.76
13.8
CCR7
CD45RO
Pre co-culture
(%) CD8+ CD19 CAR-T-cell Subset
αCD3/28 IL2
HCW9206
+ NALM6 (CD19+)
2:1 E:T
TN/SCM
TCM
TEM
TTE
αCD3/28 + IL2
0.59
44.0
0.14
55.3
HCW9206
5.10
76.1
0.43
18.4
CCR7
CD45RO
Post co-culture
(%) CD8+ CD19 CAR-T-cell Subset
αCD3/28 IL2
HCW9206

1403

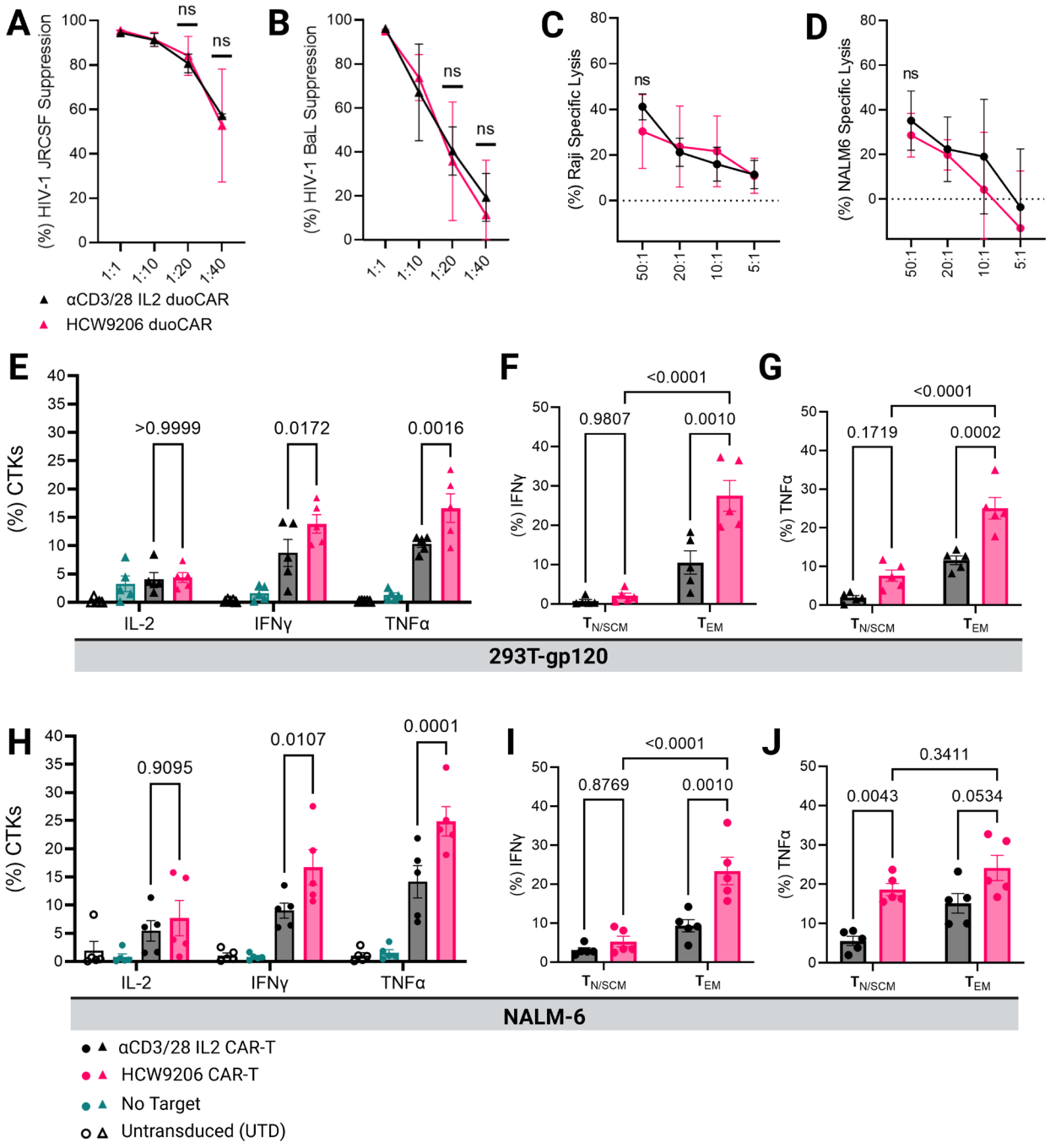
A
(%) HIV-1 JRCSF Suppression
ns
ns
1:1
1:10
1:20
1:40
αCD3/28 IL2 duoCAR
HCW9206 duoCAR
B
(%) HIV-1 BaL Suppression
C
(%) Raji Specific Lysis
50:1
20:1
10:1
5:1
D
(%) NALM6 Specific Lysis
E
(%) CTKs
>0.9999
0.0172
0.0016
IL-2
IFNγ
TNFα
F
(%) IFNγ
0.9807
<0.0001
0.0010
TN/SCM
TEM
G
(%) TNFα
0.1719
<0.0001
0.0002
293T-gp120
H
(%) CTKs
0.9095
0.0107
0.0001
I
(%) IFNγ
0.8769
<0.0001
0.0010
J
(%) TNFα
0.0043
0.3411
0.0534
NALM-6
αCD3/28 IL2 CAR-T
HCW9206 CAR-T
No Target
Untransduced (UTD)

1404

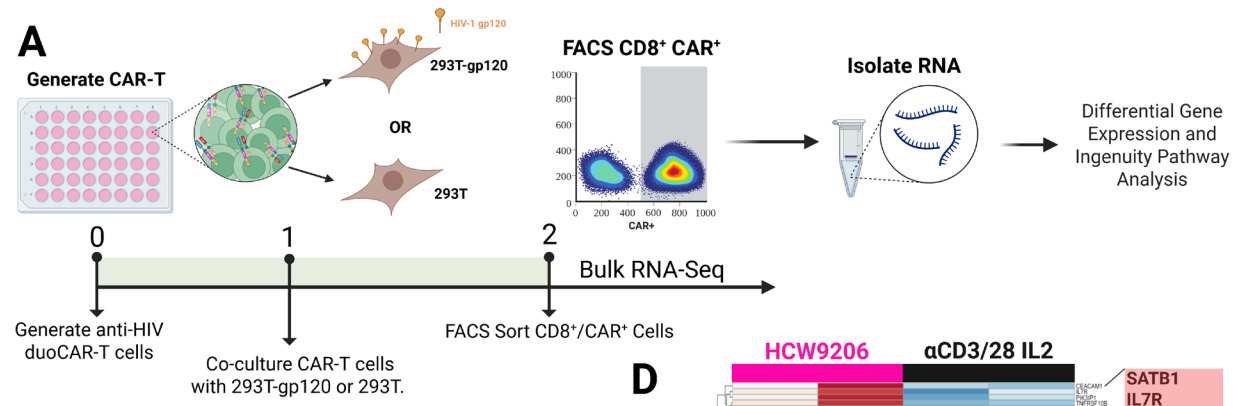
A
Generate CAR-T
HIV-1 gp120
293T-gp120
OR
293T
FACS CD8⁺ CAR⁺
CAR+
Isolate RNA
Differential Gene Expression and Ingenuity Pathway Analysis
0
1
2
Bulk RNA-Seq
Generate anti-HIV duoCAR-T cells
Co-culture CAR-T cells with 293T-gp120 or 293T.
FACS Sort CD8⁺/CAR⁺ Cells

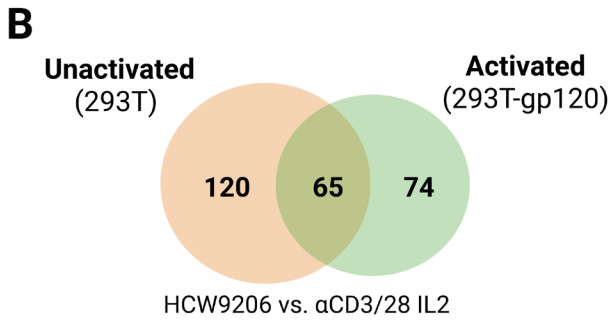
B
Unactivated (293T)
Activated (293T-gp120)
120
65
74
HCW9206 vs. αCD3/28 IL2

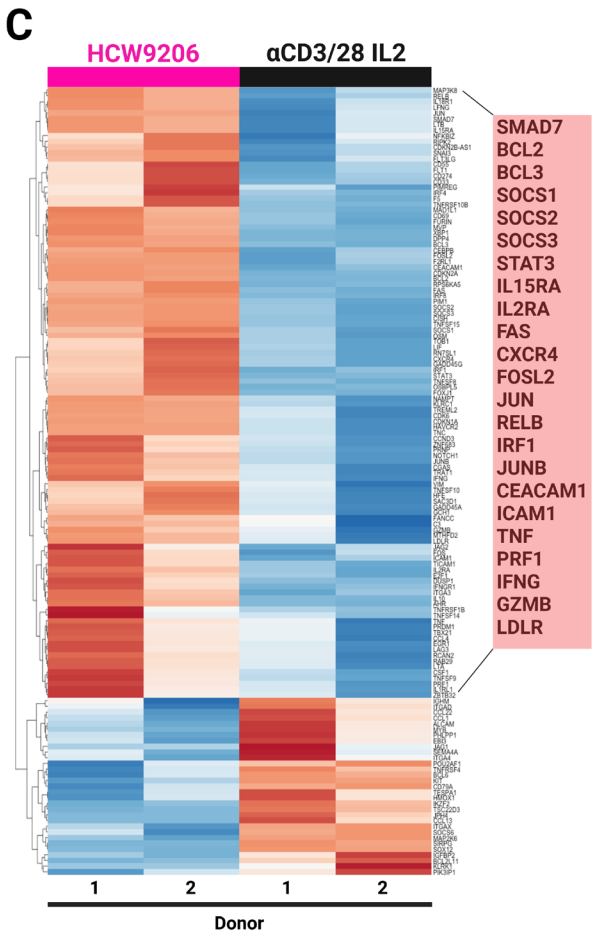
C
HCW9206
αCD3/28 IL2
SMAD7
BCL2
BCL3
SOCS1
SOCS2
SOCS3
STAT3
IL15RA
IL2RA
FAS
CXCR4
FOSL2
JUN
RELB
IRF1
JUNB
CEACAM1
ICAM1
TNF
PRF1
IFNG
GZMB
LDLR
1
2
1
2
Donor

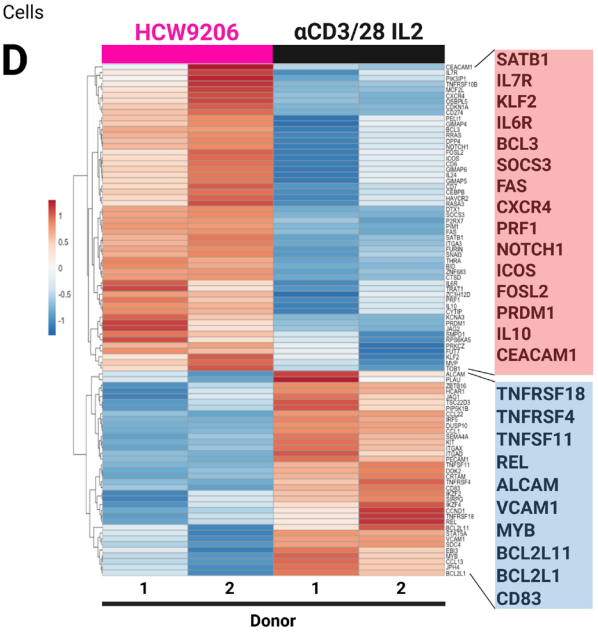
D
HCW9206
αCD3/28 IL2
SATB1
IL7R
KLF2
IL6R
BCL3
SOCS3
FAS
CXCR4
PRF1
NOTCH1
ICOS
FOSL2
PRDM1
IL10
CEACAM1
TNFRSF18
TNFRSF4
TNFSF11
REL
ALCAM
VCAM1
MYB
BCL2L11
BCL2L1
CD83
1
2
1
2
Donor

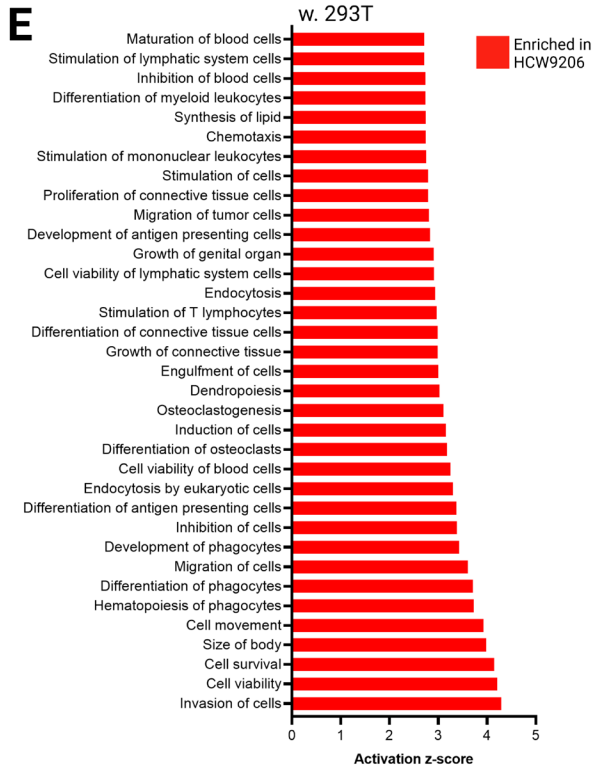
E
w. 293T
Enriched in HCW9206
Maturation of blood cells
Stimulation of lymphatic system cells
Inhibition of blood cells
Differentiation of myeloid leukocytes
Synthesis of lipid
Chemotaxis
Stimulation of mononuclear leukocytes
Stimulation of cells
Proliferation of connective tissue cells
Migration of tumor cells
Development of antigen presenting cells
Growth of genital organ
Cell viability of lymphatic system cells
Endocytosis
Stimulation of T lymphocytes
Differentiation of connective tissue cells
Growth of connective tissue
Engulfment of cells
Dendropoiesis
Osteoclastogenesis
Induction of cells
Differentiation of osteoclasts
Cell viability of blood cells
Endocytosis by eukaryotic cells
Differentiation of antigen presenting cells
Inhibition of cells
Development of phagocytes
Migration of cells
Differentiation of phagocytes
Hematopoiesis of phagocytes
Cell movement
Size of body
Cell survival
Cell viability
Invasion of cells
0
1
2
3
4
5
Activation z-score

1405

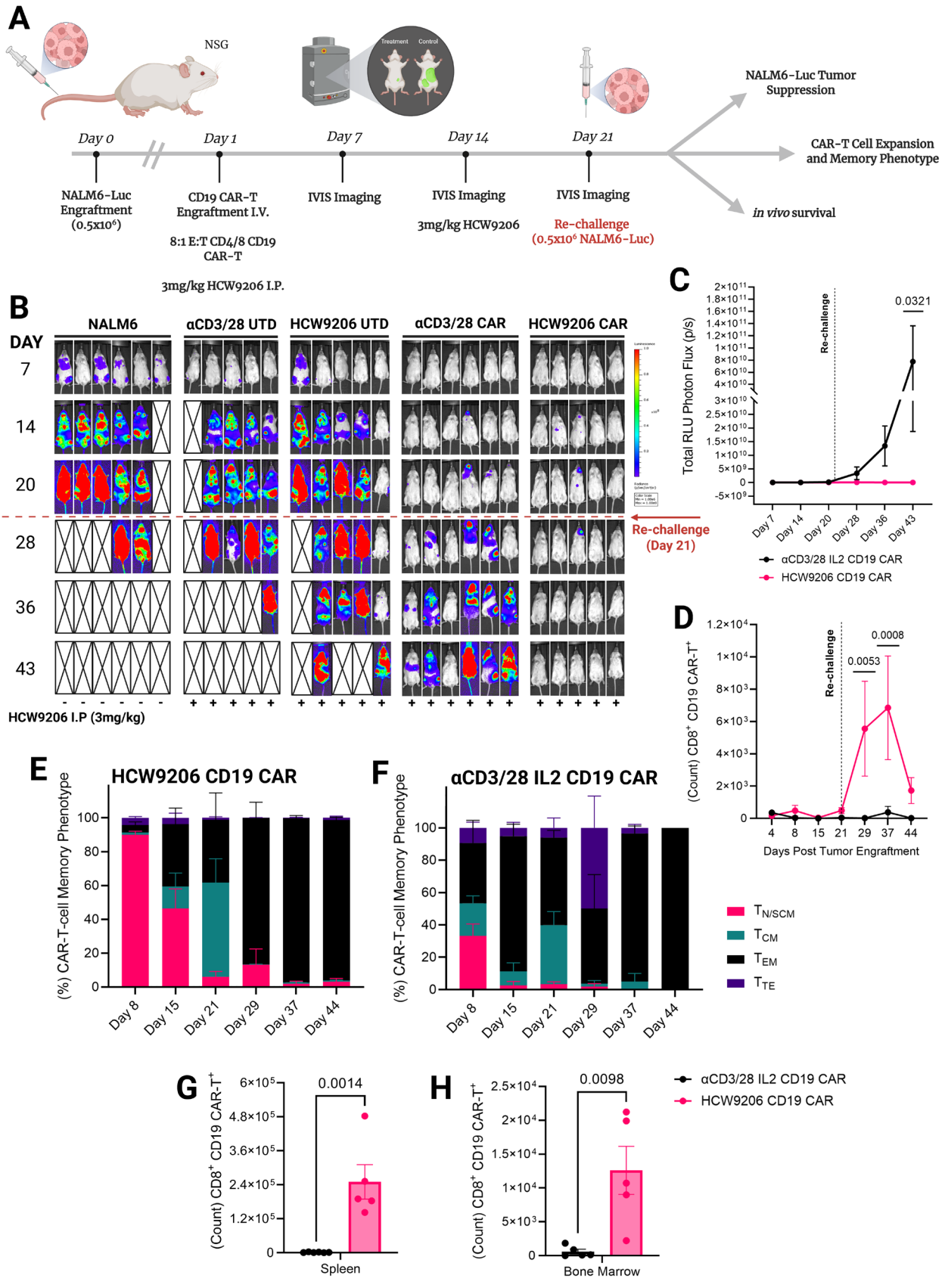
A
NSG
Treatment
Control
Day 0
Day 1
Day 7
Day 14
Day 21
NALM6-Luc Engraftment (0.5x10⁶)
CD19 CAR-T Engraftment I.V.
8:1 E:T CD4/8 CD19 CAR-T
3mg/kg HCW9206 I.P.
IVIS Imaging
IVIS Imaging
3mg/kg HCW9206
IVIS Imaging
Re-challenge (0.5x10⁶ NALM6-Luc)
NALM6-Luc Tumor Suppression
CAR-T Cell Expansion and Memory Phenotype
in vivo survival
B
NALM6
αCD3/28 UTD
HCW9206 UTD
αCD3/28 CAR
HCW9206 CAR
DAY
7
14
20
28
36
43
Re-challenge (Day 21)
HCW9206 I.P (3mg/kg)
C
Total RLU Photon Flux (p/s)
Re-challenge
0.0321
Day 7
Day 14
Day 20
Day 28
Day 36
Day 43
αCD3/28 IL2 CD19 CAR
HCW9206 CD19 CAR
D
(Count) CD8⁺ CD19 CAR-T⁺
Re-challenge
0.0053
0.0008
Days Post Tumor Engraftment
E
HCW9206 CD19 CAR
(%) CAR-T-cell Memory Phenotype
F
αCD3/28 IL2 CD19 CAR
(%) CAR-T-cell Memory Phenotype
Day 8
Day 15
Day 21
Day 29
Day 37
Day 44
T_N/SCM
T_CM
T_EM
T_TE
G
(Count) CD8⁺ CD19 CAR-T⁺
0.0014
Spleen
H
(Count) CD8⁺ CD19 CAR-T⁺
0.0098
Bone Marrow
αCD3/28 IL2 CD19 CAR
HCW9206 CD19 CAR

1406

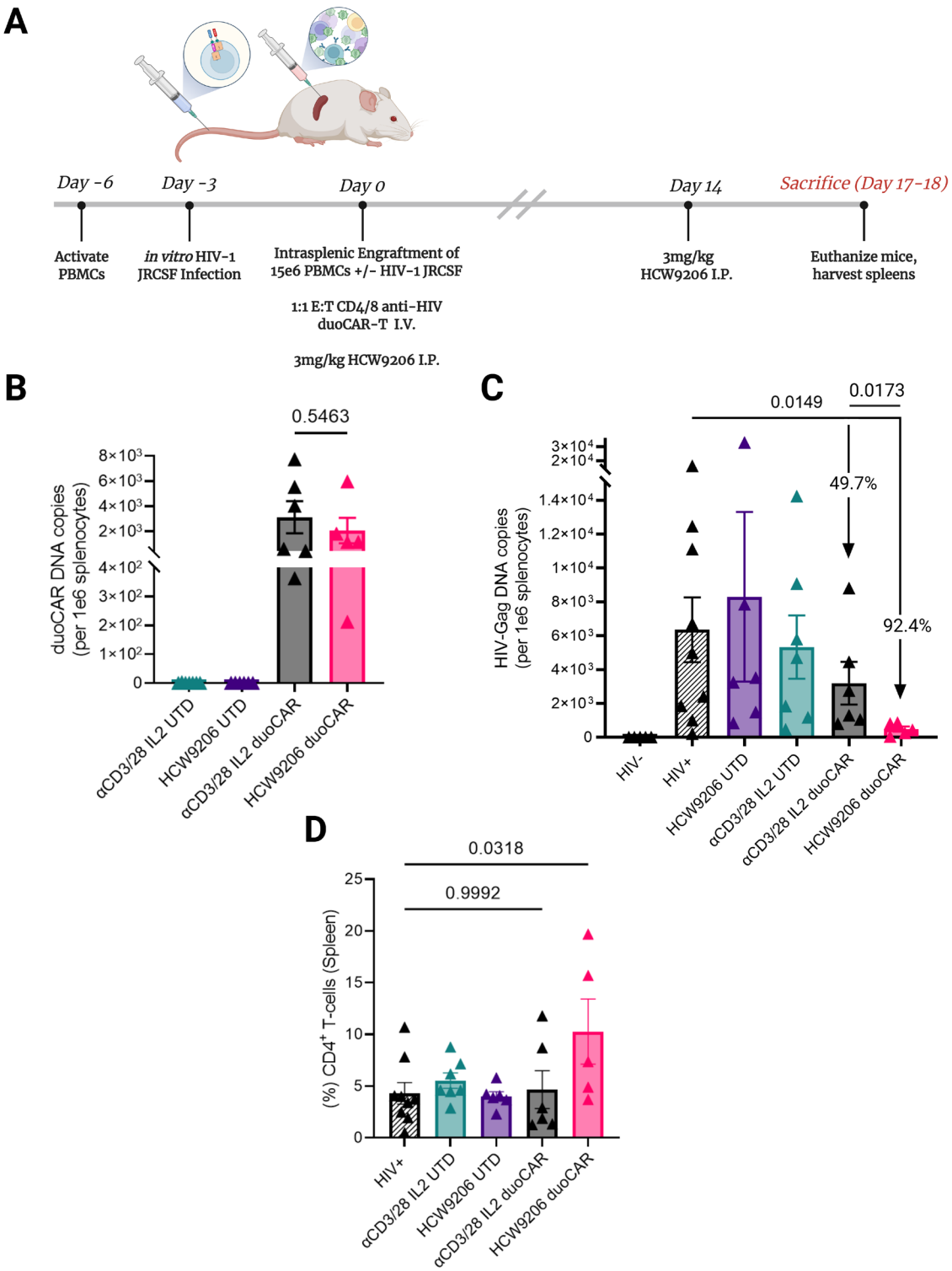
A
Day -6
Day -3
Day 0
Day 14
Sacrifice (Day 17-18)
Activate PBMCs
in vitro HIV-1 JRCSF Infection
Intrasplenic Engraftment of 15e6 PBMCs +/- HIV-1 JRCSF
1:1 E:T CD4/8 anti-HIV duoCAR-T I.V.
3mg/kg HCW9206 I.P.
3mg/kg HCW9206 I.P.
Euthanize mice, harvest spleens
B
duoCAR DNA copies (per 1e6 splenocytes)
0.5463
αCD3/28 IL2 UTD
HCW9206 UTD
αCD3/28 IL2 duoCAR
HCW9206 duoCAR
C
HIV-Gag DNA copies (per 1e6 splenocytes)
0.0149
0.0173
49.7%
92.4%
HIV-
HIV+
HCW9206 UTD
αCD3/28 IL2 UTD
αCD3/28 IL2 duoCAR
HCW9206 duoCAR
D
(%) CD4+ T-cells (Spleen)
0.0318
0.9992
HIV+
αCD3/28 IL2 UTD
HCW9206 UTD
αCD3/28 IL2 duoCAR
HCW9206 duoCAR

1407

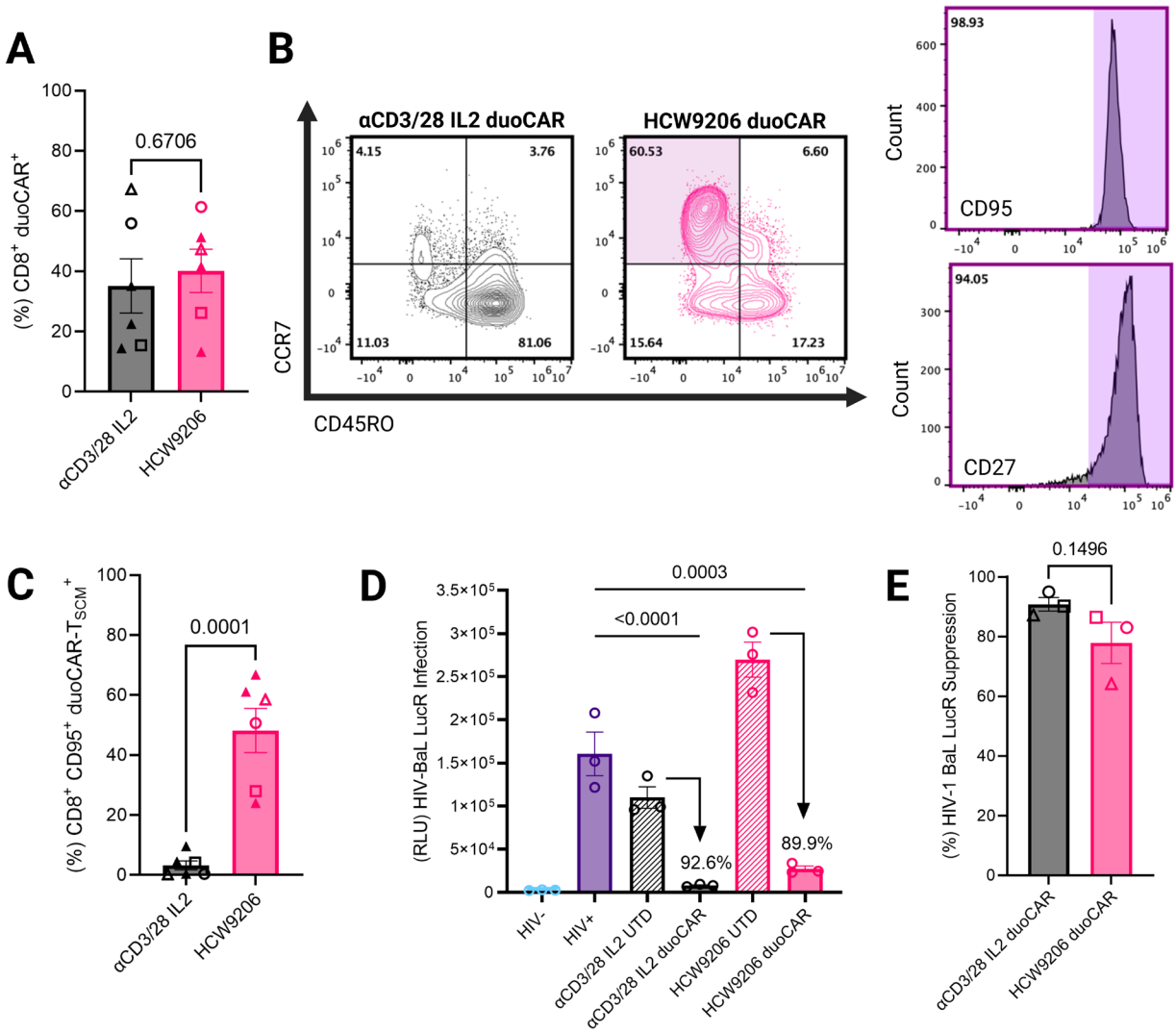
A
B
C
D
E
(%) CD8+ duoCAR+
0.6706
αCD3/28 IL2
HCW9206
αCD3/28 IL2 duoCAR
HCW9206 duoCAR
CCR7
CD45RO
4.15
3.76
11.03
81.06
60.53
6.60
15.64
17.23
Count
CD95
98.93
CD27
94.05
(%) CD8+ CD95+ duoCAR-TSCM+
0.0001
(RLU) HIV-BaL LucR Infection
0.0003
<0.0001
92.6%
89.9%
HIV-
HIV+
αCD3/28 IL2 UTD
αCD3/28 IL2 duoCAR
HCW9206 UTD
HCW9206 duoCAR
(%) HIV-1 BaL LucR Suppression
0.1496

1408